AD-A070 017 NEBRASKA UNIV LINCOLN DEPT OF ELECTRICAL ENGINEERING F/G 20/12
ELECTRICAL PROPERTIES OF THIN GAAS FILMS DEPOSITED BY SPUTTERIN--ETC(U)
MAY 79 R J SOUKUP AFOSR-77-3155

UNCLASSIFIED AFOSR-TR-79-0724 NL

| OF |
AD
A070017

END
DATE
FILMED
7-79
DDC

UNCLASSIFIED
SECURITY CLASSIFICATION OF THIS PAGE (When Data Entered)

LEVEL II

REPORT DOCUMENTATION PAGE

READ INSTRUCTIONS BEFORE COMPLETING FORM

1. REPORT NUMBER: AFOSR-TR-79-0724	2. GOVT ACCESSION NO. / 3. RECIPIENT'S CATALOG NUMBER
4. TITLE (and Subtitle): Electrical Properties of Thin GaAs Films Deposited by Sputtering.	5. TYPE OF REPORT & PERIOD COVERED: Final, 1 Oct. 1976-31 March 1979
	6. PERFORMING ORG. REPORT NUMBER
7. AUTHOR(s): Rodney J. Soukup	8. CONTRACT OR GRANT NUMBER(s): AFOSR-77-3155
9. PERFORMING ORGANIZATION NAME AND ADDRESS: University of Nebraska-Lincoln, Department of Electrical Engineering, Lincoln, Nebraska 68588	10. PROGRAM ELEMENT, PROJECT, TASK AREA & WORK UNIT NUMBERS: 2306/B2, 61102F, B2
11. CONTROLLING OFFICE NAME AND ADDRESS: AFOSR/NE, Bldg. 410, Bolling AFB, D.C. 20332	12. REPORT DATE: 31 May 1979
	13. NUMBER OF PAGES: 66
14. MONITORING AGENCY NAME & ADDRESS (if different from Controlling Office): Final rept. 1 Oct 76-31 Mar 79	15. SECURITY CLASS. (of this report): UNCLASSIFIED
	15a. DECLASSIFICATION/DOWNGRADING SCHEDULE

16. DISTRIBUTION STATEMENT (of this Report)

Approved for public release; distribution unlimited. (12) 68p.

17. DISTRIBUTION STATEMENT (of the abstract entered in Block 20, if different from Report)

DDC RECEIVED JUN 18 1979 C

18. SUPPLEMENTARY NOTES

19. KEY WORDS (Continue on reverse side if necessary and identify by block number)

Sputtering
Thin Films
Gallium Arsenide
Reflection electron diffraction
Schottky barriers
Circuit models
Impedance measurements
Capacitance-voltage measurements
Current-voltage measurements
van der Pauw measurements

20. ABSTRACT (Continue on reverse side if necessary and identify by block number)

Thin GaAs films have been deposited by sputtering with co-sputtering of As and impurity targets. These films have been deposited onto n-type GaAs substrates for Schottky barrier measurements and Cr-doped semi-insulating substrates for conductivity and Hall effect measurements.

The measurements on Schottky barriers formed by deposition of aluminum contacts onto the films of GaAs indicated that the simple Schottky barrier model

DD FORM 1 JAN 73 1473 EDITION OF 1 NOV 65 IS OBSOLETE

UNCLASSIFIED
SECURITY CLASSIFICATION OF THIS PAGE (When Data Entered)

401 033 LB

AD A070017

DDC FILE COPY

20.

does not hold for these films. An analysis of the capacitance-voltage characteristics of this device is presented and leads to a small signal model consisting of two parallel RC circuits in series. Further analysis of this circuit results in a determination of the electrical properties of the thin films.

Measurements of conductivity and Hall effect were made via the van der Pauw technique. The results prove that Si doped films are n-type and Mg doped films are p-type. The carrier concentrations are lower than expected from the intended impurity concentrations and the carrier mobility is lower than desired for device quality films. Both results indicate a deep lying trap state in the forbidden energy gap. The cause of these states is not known for sure and studies are continuing. These results are several orders of magnitude improvement over previous results.

TABLE OF CONTENTS

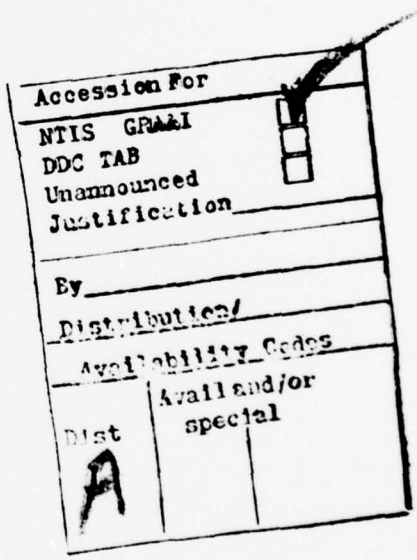

LIST OF TABLES

I. INTRODUCTION

Thin semiconducting films of GaAs have been deposited by supported plasma co-sputtering of high purity (undoped) GaAs polycrystalline targets and high purity As and Mg, and ultrahigh purity Si targets. The As is used to create a beam of excess As in order to increase the probability of depositing stoichiometric GaAs [1]. The Mg is a p-type dopant and Si an n-type dopant in these films.

The major studies of the deposited films were of two types. In one case the films were deposited onto n-type and n^+-type GaAs substrates with a Schottky barrier contact made to the film and an ohmic contact to the back of the substrate. The other studies were of films deposited onto Cr-doped, semi-insulating GaAs substrates.

The measurements made in the Schottky barrier studies were:

1) current-voltage for forward and reverse bias as a function of temperature,
2) capacitance-voltage for reverse bias at a frequency of 1 kHz and 1MHz as a function of temperature,
3) complex impedance from 5Hz to 500 kHz as a function of temperature, and
4) electron beam induced currents.

These measurements led to a circuit model which accurately describes the device. The element values are related to the properties of the thin GaAs films and these element values are determined from these measurements. Thus, this method is used as an indirect measure of the GaAs thin film electrical properties.

Studies made on the films deposited onto semi-insulating GaAs substrates consisted of measurements of conductivity and Hall effect using the van der Pauw [2] technique. The results of these measurements have led to a more direct method of determining the important semiconductor parameters of carrier mobility and concentration.

Both studies are described and explained in the following sections.

II. SCHOTTKY BARRIER STUDIES

The experimental techniques used in the fabrication of the thin films under study were presented in great detail in the previous report [3]. Only major modifications in these techniques will be described here.

A. Thin Film Fabrication

The GaAs films were deposited onto the GaAs substrates at a rate of approximately 3 $\mathring{A}$/sec. The GaAs target was changed to a target of ultrapure polycrystalline material and was water cooled to minimize sublimation of As. The substrates were maintained at a constant temperature of 520°C.

During the fabrication of the samples reported in the previous reports, a constant flow of high purity Ar was maintained by opening the sorption pump valve to maintain a desirable pressure (3×10^{-3} Torr). A mass spectrometer was attached to the vacuum system to check the background and sputter gas purity.

It was observed that excess amounts of oxygen entered the system from the sorption pump. Hence, it was decided to close the sorption pump value completely and open the ion pump poppet valve to maintain a constant pressure with a continuous flow of Ar during deposition. The mass spectrometer analysis at background pressure, after admitting and further cleaning the Ar, and after depositing the samples, are shown in Figures 1, 2,and 3 respectively. The background was found to contain barely detected quantities of H_2O and CO. Only minute impurity gases were detected in the Ar gas. A high energy reflection electron diffraction gun and screen were installed to determine substrate surface crystal quality, after pre-vacuum and vacuum preparation, and the film crystal quality.

The substrates were cleaved from single crystal GaAs wafers. The n-type substrates were Se doped while the p-type substrates were Zn doped. The pre-vacuum preparation consisted of a methanol ultrasonic cleaning and etching in both bromine-methanol and a caros etch. The details have been described in the previous

report [3].

During deposition the substrates were held at a constant temperature of 520°C and films were grown to thicknesses between 1 μm and 2.5 μm. Table I lists the various samples, substrates, deposition conditions, and electron diffraction results. Metallization was done both in-situ before removal from the UHV system and after removal in a diffusion pumped vacuum system. Ohmic contacts were made by evaporation of a thin layer of In followed by more than 1 μm of Al as described by Healy and Mattauch [4]. Schottky barriers were formed by deposition of aluminum on the surface and contacts were defined by conventional photolithography techniques. The samples were bonded into hybrid packages for convenient measurements using commercial test fixtures. The contact pads were connected to the packages by thermo-compression bonding of gold wires between the samples and the package leads.

B. Experimental Results

The types of measurements made on these samples were described in the introduction. A short description of some of these results is presented here.

1. Current-Voltage (I-V) Characteristics

The I-V characteristics of several samples are shown in Figures 4, 5, and 6. Figure 4 depicts these characteristics for Schottky barriers deposited directly onto n-type substrates under different conditions in order to establish a basis for comparison. Curve 1 is data obtained from a sample in which the Al metallization was deposited onto a substrate cleaned, as described, immediately after cleaning, while the substrate was still hot. The result was an Al-GaAs ohmic contact. Curve 2 shows the data obtained from a sample in which the metallization was deposited in UHV after cooling the substrate. Curves 3 and 4 show the data from samples which were removed from the UHV system, exposed to the atmosphere, and metallized in a diffusion pumped system. The presence of an oxide layer between the metal and GaAs appears to improve the Schottky-

TABLE I

Samples and Growth Parameters

Sample No.	Substrate Type	Deposition* Parameters	RED Results	Metallization Parameters
7-1	1	No Film	Good	a
9-1	1	No Film	Fair	b
12-4	1	No Film	Good	c
15-4	2	No Film	None	c
12-1	1	1μm, undoped	Fair	c
13-1	1	2.5μm, undoped	Good	c
11-4	1	1μm, 1% Si	Poor	b
11-1	1	1μm, 100% Si	Fair	b
12-2	1	1μm, 100% Si	Poor	c
15-2	2	1.8μm, 100% Si	Fair	c
12-3	1	1μm, 100% Mg	Poor	c
13-4	1	2.5μm, 100% Mg	Fair	c
8-3	3	1μm, 100% Mg	Poor	b

*The percentage refers to the on-time duty cycle of the pulsed impurity target voltage.

SUBSTRATE TYPES: 1) Se doped, n-type, $N_d=10^{18}/cm^3$, 2) Undoped, n-type, $N_d=4x10^{16}/cm^3$, 3) Zn doped, p-type, $N_a=2.2x10^{18}/cm^3$.

METALLIZATION PARAMETERS: a) Al on hot (520°C) GaAs, b) Al on room temperature GaAs in UHV, c) Al on GaAs exposed to atmosphere.

barrier I-V characteristics. The reverse "breakdown" voltage is strongly dependent on the substrate doping concentration, being much higher for the lighter doped substrates, as expected. Figure 5 shows the I-V characteristics on three different samples which were deposited on n-type substrates. The strong dependence of the reverse "breakdown" voltage on doping of the samples is evident again. Figure 6 compares the I-V characteristics of samples doped with Mg and Si on n-type and p-type substrates. Curve 2 is data for an Mg doped film on an n-type substrate. This sample has the highest reverse "breakdown" voltage ($\simeq$ 10V) of all samples measured. The Mg doped films are p-type (see section III) and therefore this curve is that of the I-V characteristics of a p-n junction, rather than a metal-semiconductor diode. Curve 3 is for a Mg doped film deposited onto a p-type substrate. The polarity for forward bias is opposite that for n-type samples, as is expected for a p-type Schottky barrier. These results were the first indication that Mg doped films are actually p-type. The I-V characteristics for each sample were made over a wide range of temperature in order to determine the barrier height. The barrier heights determined from these measurements are presented in Table II.

2. Capacitance-Voltage (C-V) Characteristics

The capacitance of these samples was measured as a function of bias voltage at 1 kHz and at 1 MHz using automatic, digital capacitance bridges. These measurements were also made as a function of temperature. Figures 7 and 8 show the capacitance versus bias voltage measured at 1 MHz and 1 kHz, respectively, for four different samples. In three samples the capacitance decreases with increasing reverse bias as expected for a Schottky contact. However, in one case the capacitance is independent of the reverse bias voltage.

3. Complex Impedance-Frequency (Z-f) Characteristics

The magnitude of the impedance $|Z|$, and the phase angle θ of these device

TABLE II

Results of Schottky Barrier Measurements

Sample	a ϕ_{b1}(eV)	b ϕ_{b2}(eV)	c ψ(eV)	d σ(℧/cm)	N_d(cm^{-3})
7-1	-	-	-	-	-
9-1	0.32	0.29	-	-	-
12-4	0.46	0.33	-	-	$1x10^{18}$
15-4	-	0.66	-	-	$3.6x10^{16}$
12-1	0.46	0.40	0.44	$7.11x10^{-7}$	$8.4x10^{16}$
13-1	0.42	-	0.23	$6.08x10^{-6}$	$7.1x10^{16}$
11-4	0.60	0.47	0.28	$5.38x10^{-7}$	$4.5x10^{16}$
11-1	0.45	0.42	0.27	$2.27x10^{-6}$	$5.7x10^{18}$
12-2	0.73	-	0.34	$1.61x10^{-6}$	-
15-2	0.46	0.39	0.16	$1.86x10^{-6}$	-
12-3	0.69*	0.66*	0.21	$4.0x10^{-7}$	$1.9x10^{17}$
13-4	-	0.70*	-	$1.1x10^{-6}$	-
8-3	-	-	-	-	-

a: Schottky barrier height,
Evaluated from R_{SB} versus temperature.

b: Schottky barrier height,
Evaluated from I-V characteristics.

c: Bulk activation energy,
Evaluated from R_B versus temperature.

d: Conductivity,
Evaluated from R_B and C_B at T = 303°K

*Built in junction potential, not Schottky barrier height.

structures were measured as a function of frequency at different temperatures. Figure 9 is a plot of the impedance phase angle as a function of frequency for a number of samples. It can be seen that the undoped film and the lightly Si doped films have a minima and maxima as a function of frequency while the Mg doped film on n-type substrate and the Schottky-barrier formed directly on the substrate do not exhibit any structure in the curves. Figure 10 is a plot of the magnitude of the impedance as a function of frequency for a number of samples.

C. Analysis of Schottky Barrier Results

1. Analysis of Complex Impedance as a Function of Frequency.

Figure 11 shows the energy band diagram and the circuit model deduced in the analysis of the results. C_{SB} and R_{SB} are the Schottky-barrier capacitance and resistance respectively, C_B and R_B are respectively the capacitance and resistance of the bulk (film) region, and C_{LH} and R_{LH} are capacitance and resistance of low-high (n-n^+) junction. For the n-n^+ junction it is assumed that $R_{LH} = 0$, see Appendix B. In this case C_{LH} is shorted and the circuit model is simply two parallel RC circuits in series. It is shown by network analysis that this kind of a circuit model may lead to a minima and a maxima in the phase angle versus frequency curve, see Appendix A.

The component values R_{SB}, C_{SB}, R_B, and C_B can be evaluated from measurements of the phase angle and magnitude of the impedance as a function of frequency. The series resistance is given in Appendix A as eqn. (A-4) and is repeated here:

$$R_s = R_{SB} + R_B \quad . \tag{1}$$

The magnitude of the impedance is eqn. (A-2) and is:

$$|Z| = R_s \left[\frac{1 + \omega^2 R_p^2 C_p^2}{(1+\omega^2 R_{SB}^2 C_{SB}^2)(1+\omega^2 R_B^2 C_B^2)} \right]^{1/2} \quad .$$

It can be seen that a measure of R_s is the low frequency value of the impedance magnitude, i.e.

$$R_s = \lim_{\omega \to 0} |Z| \quad . \tag{3}$$

The series capacitance can be determined by a measure of the high frequency equivalent capacitance, Appendix B is an analysis of this capacitance. The capacitance measured by a bridge is the equivalent parallel capacitance, C_{par} and is given in eqn. (B-25),

$$C_{par} = \frac{R_{SB}^2 C_{SB} + R_B^2 C_B + \omega^2 R_{SB}^2 R_B^2 C_{SB} C_B (C_{SB} + C_B)}{(R_{SB} + R_B)^2 + \omega^2 R_{SB}^2 R_B^2 (C_{SB} + C_B)^2} \tag{4}$$

At high frequency

$$C_{par\infty} = \lim_{\omega \to \infty} C_{par} = C_{SB} C_B / (C_{SB} + C_B) \ , \tag{5}$$

which is just

$$C_S = C_{SB} \, C_B / C_p , \tag{6}$$

as in eqn. (A-7). Knowing R_S, C_S and the frequencies f_1 and f_2 at which θ reaches a minima and maxima respectively, the component values can be determined. The calculated and measured values of $|Z|$ and θ for one typical sample at four different temperatures are shown in figures 12 and 13 respectively. The agreement between the theory and experiment was not very good for certain samples at certain temperatures. This disagreement between theory and experiment is attributed to the approximations made in determining the frequencies at which minima and maxima occur in the phase angle. The variation of the phase angle at minima and maxima was extremely slow, hence it was not possible to determine these frequencies with any accuracy.

As a consequence of this discrepancy a second method of analysis was carried out. The impedance phase angle is given by eqn. (A-3) and is

$$\theta = \tan^{-1} \omega R_p C_p - \tan^{-1} \omega R_B C_B - \tan^{-1} \omega R_{SB} C_{SB} \ . \qquad (7)$$

At low frequencies $\omega R_{SB} C_{SB}$ is very large compared to $\omega R_p C_p$ or $\omega R_B C_B$. In this case θ_L is given by eqn. (A-10),

$$\theta_L \simeq - \tan^{-1} \ R_{SB} C_{SB} \ , \qquad (8)$$

and $T_{SB} = R_{SB} C_{SB}$ is determined. Knowing the series resistance R_S and series capacitance C_S, the product $R_p \ C_p$ can be expressed in terms of $R_B C_B$, see eqn. (A-8). The result is

$$R_p C_p = T_p = \frac{T_{SB} T_B}{T_S} = R_B C_B \ \frac{T_{SB}}{T_S} \qquad (9)$$

where T_{SB} and T_S are now known. The best value of $R_B C_B$ to fit the phase angle is determined by computer methods. The computer program is shown in Appendix C. Evaluating the component values, the calculated values of θ versus observed values are plotted for one sample in Fig. 14. The RMS error in θ varies from 1.0° to 3.6° in the temperature range T = 313°K to T = 370°K. Considering that the impedance meter is accurate to $\pm$ 6°,this is exellent agreement. The agreement between theory and experiment is better using the second method than the first method. Table III shows the values of R_{SB}, C_{SB}, C_B and R_B for this sample. The temperature dependence of R_{SB} is used to determine the Schottky-barrier height ϕ_{b1} and the temperature dependence of R_B yields ψ, the activation energy of carriers in the film. The conductivity σ of the semiconductor is determined from the values of R_B and C_B at a particular temperature. These values of ϕ_{b1} and σ are listed in Table II.

2. Capacitance-Voltage Characteristics Analysis

An analysis of the capacitance vs reverse bias voltage for the device under study here is made in Appendix B. The resulting capacitance as measured by a bridge is given in eqn. (4). The measured capacitance may be independent

TABLE III

Component Values Determined For

Sample 12-1

T	313°K	323°K	333°K	345°K	357°K	370°K
R_{SB} (kΩ)	69.764	40.815	23.860	13.113	7.33	3.66
R_B (Ω)	236	185	140	87	70	40
C_{SB} (nF)	6.452	6.547	6.643	7.408	7.053	7.142
C_B (nF)	2.491	3.216	3.684	4.109	5.813	8.193

Calculated and measured values of capacitance at 1 kHz and at 1 MHz

	f = 1 kHz		f = 1 MHz	
T	C_{cal} (nF)	C_{meas} (nF)	C_{cal} (nF)	C_{meas} (nF)
313°K	6.41	6.23	1.823	2.010
323°K	6.49	6.40	2.190	2.156
333°K	6.57	6.53	2.421	2.369
345°K	7.94	*	2.837	2.720
357°K	6.92	*	3.302	3.200
370°K	6.99	*	4.020	3.820

*Could not be measured.

of voltage or depend on voltage in a complicated manner as described in Appendix B. This capacitance may also depend on temperature, depending on the values of R_{SB}, C_{SB}, R_B, and C_B. The capacitance values C_{SB} and C_B at V_a=0 have been determined from the |Z|and θ frequency dependent curves for a few samples. An attempt is being made to determine the individual voltage dependence of C_{SB} and C_B. The calculations are incomplete at this time. The $\frac{1}{C^2}$ vs V curves did yield straight lines typical of a Schottky barrier, for samples which exhibited no structure in the θ versus frequency curves. These plots are shown in Figure 15. The values of doping concentrations (N_d) determined from these curves are also given in Table II.

3. Current-Voltage Characteristics

No detailed analysis of the I-V curves has been made at this time. However, these curves are also not typical of standard Schottky barriers.

III. CONDUCTIVITY AND HALL EFFECT STUDIES

A. Vacuum System Description

There have been a number of improvements made to the Ultek TNB-X vacuum system used for these studies during this period. Only the changes will be described here. The reader may refer to an earlier report [3] for other system details. The vacuum system itself has been upgraded with the installation of a complete set of eight new differential ion pump elements. This gives a pumping speed of 200 liters/sec and a base pressure of 1×10^{-10} Torr, after baking at 125°C.

A Reflection Electron Diffraction (RED) system has been installed to replace the LEED system used previously. The RED system consists of a commercial 3K/5U electron gun mounted on the 8" flange opposite the viewing window. The associated power supply is shown in Fig. 16. A 3" diameter phosphor coated screen is mounted in the top center of the viewing window. The electron energy

used is 2.5 keV. This system has been quite successful as many diffraction patterns have been observed from substrates and films.

A model Spectramass 80 residual gas analyzer has been installed to provide for detailed monitoring of the gas environment in the system and features a mass detection range of 2 to 80 atomic mass units.

A special holder was fabricated for one titanium sublimation filament to be inserted into the main vacuum chamber through one of the 1 1/2" instrumentation ports. This allows for the deposit of a Ti layer on the lower section of the main chamber, above the poppet valve for better pumping. It was tested and found to be very effective in pumping any oxygen or nitrogen contamination.

The main GaAs target is now supported on a 1" diameter water-cooled platform. This is connected to a ceramaseal flange with two electrically insulated 1/4" tube feedthroughs so that the target voltage can be connected directly to the platform.

A plasma source to be used for sputter cleaning of the sample was fabricated from an ion gauge tube and mounted on the top flange of the vacuum chamber. The emission filament is grounded and the helical grid is biased at approximately +100 volts.

There has been considerable improvement made in the substrate holder and manipulation facilities during this period. Figure 17 shows the apparatus used for most of these studies. The most important change is the Ultek Model 283-8550 XYZ manipulator which allows great flexibility in the positioning of the sample. There are two primary positions used. One is with the sample facing upward and raised so that the RED system can be used. The second is with the sample facing down and lowered into a hole in a shield plate which separates the plasma volume from the upper portion of the vacuum chamber.

This shield plate was incorporated to prevent unwanted deposition on more than one sample at a time and functions as a shutter, since the sample must be in line with and lowered into the hole for deposition to begin.

The vacuum side of the flange in Figure 17 also incorporates several improvements. The flexible wires are now an in-house version similar to those available from Ceramaseal and have proven to be more reliable than the simple bead covered wires. This system has an additional braided sheath over the beads and the cross-shaped ceramic anchor point so that the leads which actually connect the substrate holder are stationary. The final sample holder shown in Figure 18 was designed to hold 3 samples to allow more movement in the vertical direction; the shield plate mentioned earlier restricted that movement. The new holder also is more rigid than before and maintains a consistent sample alignment. The molybdenum block is now made of three pieces. When the top piece, to which the GaAs sample is bonded, is removed, the heater filament is not disturbed. This has enhanced the reliability and longevity of the substrate heaters considerably. The thermocouple is now welded to the washer used on the screw which holds the top Mo piece to the heater block. This places it in good thermal contact with the top piece and quite close to the substrate for accurate temperature measurement of the substrate during annealing, cleaning, and deposition.

B. Sample Preparation

The chemical etching procedure used to prepare the substrates was simplified by the elimation of the Bromine-Methanol etch. The procedure used is an ultrasonic cleaning in reagent grade methanol for 5 minutes, a rinse in deionized water, an etch in a freshly prepared Caros etch (1:1:5 of H_2O: H_2O_2:H_2SO_4), and a rinse in deionized water until they were blown dry with dry nitrogen and fastened to the Mo holder. Insertion into the vacuum system, pumpdown, and bakeout were done as previously described.

The substrates were checked for a RED pattern before in-vacuum cleaning and only rarely exhibited a diffraction pattern. When there was a pattern it was poor. On the basis of information from other researchers [1] it was decided that sputter cleaning should become a regular part of the pre-deposition procedure. Many different combinations of sample bias voltage, sample electron current, time and concurrent anneal temperature were tried. The effectiveness of each was judged from the RED pattern taken after each cleaning. The most effective combination was found to be: -100v, 300 μa, 5 minutes and 350°C, respectively. The argon pressure was 5×10^{-4} Torr during sputter cleaning. This procedure nearly always yielded a fair or good RED pattern indicative of a single crystal GaAs substrate surface.

After the sputter cleaning, the argon and any contaminants released during the cleaning were pumped out with the ion pump. After the RED pattern had been checked, fresh argon was admitted to a pressure of 2×10^{-3} Torr for deposition. The residual gas analyzer proved its worth by detecting the presence of oxygen contamination in the argon gas whenever the sorption pump was used to provide argon flow during deposition. Oxygen acts as a deep lying impurity energy level and can be used as a compensation dopant

to produce semi-insulating GaAs. Hence it was clearly undesirable. Therefore, the metal-sealed bakeable valve which separates the sorption pump from the main chamber now remains closed after bakeout. Some argon throughput is still maintained by slightly opening the poppet valve to the ion pump during deposition. A pressure of 1×10^{-6} Torr is maintained in the pump. This results in a time of 10 minutes for a complete change of the argon.

An arsenic subtarget was added between sets 21 and 22 because of Arthur's finding [1] that better stoichiometry is achieved when there is excess arsenic in the molecular beam, in molecular beam epitaxy studies. This target was always sputtered continuously, at first biased at -300 volts like the other dopant targets but later connected to the main GaAs target at -600v dc.

The targets were always presputtered for 10 minutes with the sample shielded. The sample was then moved into deposition position, lowered into the hole in the shield plate, and the film was deposited. The rate was always about 4 $\mathring{A}$/sec. The argon was pumped out again and RED studies of the film were made.

The electrical contacts to all samples in sets 17 through 24 were made with a thin In layer covered by a thick Al layer, as previously reported [3]. These did not, however, appear to yield good ohmic contacts to all the samples. Thus, it was decided to substitute tin as the thin layer on future n-type samples and magnesium on future p-type samples. These elements are both standard dopants for GaAs and have high diffusion constants. It was therefore expected that they would easily form the n^+ or p^+ contact layer which is required for good ohmic contact. Only the

two latest sets (25 and 26) have been fabricated in this manner, but this technique appears very promising.

C. Electrical Measurement Techniques (van der Pauw)

The resistivity and Hall Effect measurements techniques have also been improved considerably during this period. The first change was to go to a standard van der Pauw geometry [6] for thin film work. The resistivity determination requires the measurement of two pseudo resistances, defined as:

$$R_{AB,CD} = \frac{V_D - V_C}{I_{AB}} , \tag{10}$$

where V_D and V_C are the potentials at points D and C when current I_{AB} enters at point A and leaves at point B. Similarly:

$$R_{BC,DA} = \frac{V_A - V_D}{I_{BC}} . \tag{11}$$

A standard form has been developed for the resistivity and Hall effect data; it is shown in Table IV with typical results. The two resistances are referred to simply as R_1 and R_2. The R_1/R_2 column is actually slightly ambiguous because it is actually R_1/R_2 or R_2/R_1, whichever is greater than one. The mathematical relation between the resistance ratio and factor "f" is transcendental. Therefore, it has been solved numerically and a chart prepared to obtain the "f" factor to three decimal places. The resistivity is then found from:

$$\rho = \frac{\pi d}{\ln 2} \times \frac{R_1 + R_2}{2} \times f$$

$$= 2.2662d\,(R_1 + R_2)f \text{ (ohm - cm)}, \tag{12}$$

where d is the thickness of the film in cm.

TABLE IV

DC van der Pauw Measurement
Data Form

Sample 26-B

Date 3/12/79

Substrate semi-insulating

Operator E.F.

Dopant 100% Si with 100% As

Thickness 2×10^{-4} cm

Deposition comments: T = 450° C

Cable → / Temp	V_1(V)	I_1	V_2(V)	I_2	R_1(Ω)	R_2(Ω)	R_1/R_2	f	ρ(Ω-cm)
22°C	1.122	1 mA	1.404	1 mA	1122	1404	1.251	.996	1.140
29.9°C	.9976	↓	1.240	↓	997.6	1240	1.243	.997	1.011
39.4°C	.8675		1.070		867.5	1070	1.233	.996	.875
49.4°C	.7430		.9150		743.0	915.0	1.231	.996	.748
60.2°C	.6410		.7843		641.0	784.3	1.224	.997	.644
71.7°C	.5525		.6736		552.5	673.6	1.219	.997	.554
84°C	.4761		.5770		476.1	577.0	1.212	.997	.476
97.2°C	.4075	↓	.4905	↓	407.5	490.5	1.204	.997	.406

ϕ = .131

Magnet current: 5.8 amp $\vec{B}$: 2000 gauss

cable → [B] [A]

	I_s^+	V_s^+	R^+	I_s^-	V_s^-	R^-	n-type	p-type
B°	1 mA	-.2618V	-261.8Ω	1 mA	.2615V	261.5Ω	if $\Delta R^+ > 0$	if $\Delta R^+ < 0$
B^+	↓	-.2438V	-243.8Ω	↓	.2436V	243.6Ω	if $\Delta R^- < 0$	if $\Delta R^- > 0$
B^-		-.2788V	-278.8Ω		.2787V	278.7Ω	(X)	( )

$\frac{1}{2}[R^+(B^+)-R^+(B^-)]=\Delta R^+=17.5\Omega$ $\frac{1}{2}[R^-(B^+)-R^-(B^-)]=\Delta R^-=-17.55\Omega$ $\Delta R=\frac{1}{2}[|\Delta R^+|+|\Delta R^-|]=17.5\Omega$

$\mu = \frac{Th \times \Delta R}{B \times \rho} \times 10^{+8} =$ 154 cm^2/volt-sec $\quad n = \frac{1}{q\rho\mu} =$ 3.57×10^{16} $/cm^3$

Comments: Excellent stability during all measurements.

The Hall effect uses a third pseudo resistance $R_{BD,AC}$. The mobility is then obtained directly from:

$$\mu = \frac{d\ \Delta R_{BD,AC}}{B\rho} \times 10^8 \quad (cm^2/volt\ sec)\ , \tag{13}$$

where $\Delta R_{BC,AC}$ is the change in $R_{BD,AC}$ when the magnetic field is applied, and B is the magnetic field in gauss. Six measurements are required, as shown in Table IV to average out other effects. Finally, the carrier concentration is found directly from:

$$n = \frac{1}{q\rho\mu}\ , \tag{14}$$

where q is the electronic charge.

The van der Pauw technique allows the use of a simple metallization pattern which can be easily made directly by evaporation through a metal mask. Hence the metal etching process which was used with previous patterns has been eliminated. The size of each sample is about 5 mm square; the contacts are on a square 3.8 mm on a side and they are 0.34 mm in diameter. The samples were cleaved on all four sides after metallization to guard against any conduction around the edge of the sample to the indium which remains on the back surface after removal from the Mo block. They were bonded into hybrid packages with Abelbond 826-1 epoxy and a thermocompression wire bonder was used for the electrical connections. A completed set of samples is shown in Fig. 19. This package is then ready for insertion into the Barnes test socket which is mounted in the temperature test oven or the magnet gap.

The Barnes sockets have been remounted so that all the required leads now come out of the oven or magnet gap on 8 shielded cables with BNC connectors. The first samples in this period were measured using a homemade

sweep generator with a Keithley 600B electrometer to measure the current. However, that has now been replaced by a Keithley 225 current source which has proven to be much easier to use. A connection box has been built into which the current source, the Hewlett-Packard 3465B voltmeter and the two BNC cables for a particular sample are plugged. Then the two different connections used for resistivity measurements and the third used for Hall effect can each be made by the setting of one switch. This keeps all leads shielded at all times and eliminates the chance for incorrect connections. The H-P 3465B digital VOM is new and has proven to be a great improvement because of its very high input impedance and superior noise rejection. This has been particularly important in the Hall effect measurements.

The Hall effect apparatus is still centered around a Cenco Model J electromagnet. However, the pole pieces have been changed to a 6 1/2 cm gap with a foam dewar mounted in the gap. The sample is held in a brass box inside the dewar, so that liquid nitrogen poured in the dewar does not touch the sample. Temperatures of approximately 100°K are easily obtained in this manner. It is planned to make measurements at temperatures between 100°K and 300°K. The field used with the setup is 2000 gauss.

Two further measurement techniques have been given rather limited use so far but will be used more as the quality of the films improves. The first is Electron Beam Induced Currents (EBIC) in the Scanning Electron Microscope (SEM). This technique uses a sample with a Schottky barrier. Hole-electron pairs are generated whenever the high energy electron beam strikes a semiconductor. If this occurs within a few diffusion lengths of a junction, some of the minority carriers generated will be collected and can be measured. Either a p-n or Schottky junction will suffice as the collection

junctions. If the SEM beam is swept toward the junction while the current is being measured, a plot can be made of the EBIC versus the distance of the pair generation from the junction. Some care must be exercised with this technique with thin films because of the high energy electron beam penetration of the sample. This distance should be less than the film thickness or the experiment will be complicated by pair generation in the substrate. The depth of penetration may be found with sufficient accuracy from [7]

$$R = \frac{1}{\rho} \; 2.76 \times 10^{-11} \; AZ^{8/9} \; E^{5/3} \quad , \tag{15}$$

where R is the range is centimeters, ρ the material density in g/cm^3, A the atomic weight, Z is the atomic number, and E is the electron beam energy in electron-volts. For GaAs with 20 KeV electron this gives a range of 2.5 microns, for 10 KeV electrons it gives 0.8 microns.

The second technique is to use the Selected Area Diffraction (SAD) made on the Cambridge S4-10 Stereoscan available in the laboratory. This technique probes the crystalline structure of the surface. The SAD mode causes the beam to be directed at the surface at different angles as it scans over the surface. If the beam direction lines up with a preferred Bragg scattering direction into the crystal, there is very little secondary electron production at that point and the image appears dark. Conversely the image will appear brighter where there is no preferred scattering into the material.Such an image is an inverse electron channeling pattern [8]. The images appear very much like Kikuchi patterns, which are transmission electron channeling patterns. The channeling pattern appears superimposed on the normal topographic image of the surface.

D. Experimental Results (van der Pauw)

There have been 32 samples made recently for van der Pauw resistivity and Hall effect testing. Table V is a summary of the deposition parameters and the electrical measurement results.

The first series of samples-sets 17 through 20 were used for two purposes. The first purpose was to check the effectiveness of different variations of the sputter-anneal pre-deposition cleaning as determined from the RED patterns, and the second to search for the optimum deposition temperature as determined from both the RED patterns and the electrical measurement results. RED was used as a qualitative tool to help in the adjustment of system parameters to obtain the best films. No attempt was made to do detailed analysis of the RED pattern to determine surface structure. The optimum sputter cleaning seemed to be found with sample 19C for which the parameters were: -100V, 300 μa, 300°C, and 20 min. The RED pattern from this substrate is shown in Fig. 20. There was some lack of reproducibility of these patterns, as can be seen from glancing over the results for later samples. This made the finding of an optimum procedure rather difficult and the procedure was changed again in set 25 to the parameters mentioned earlier under sample preparations. This change seemed to yield further improvement in the surface conditions, as can be seen in Fig. 21.

The search for the optimum deposition temperature was also made primarily on the basis of the RED patterns. On that basis samples 18D and 19A were clearly the best; the RED pattern of 19A is shown in Fig. 22. Both of these samples were deposited at 400°C, so that become the standard deposition temperature for the next several sets.

TABLE V

van der Pauw Results

Sample #	Substrate Type	Dopants	Thick-ness	Substrate Preparation V	I	Temp	Time	Reflec. Substrate	Elec. Diff. Film	Deposition Temp	Rate	Resistivity at 30°C(Ω-cm)	Activation Energy(eV)	Type	Mobility cm^2/volt-sec	Carrier Concent
17A	SI	none	1.0μm	-	-	580°C	30min	2sp=poor	4line=fair	250°C	3.7Å/s	16.3k	.68→.97	not measured		
17C	SI	none	1.0	-	-	580	36	2sp=poor	4sp=fair	300	3.82	14.2k	.63→1.48	"		
17D	SI	none	1.0	100v	3ma	144	30	1sp=poor	2sp→1n=poor	300	3.36	11.4k	1.25	"		
18A	SI	none	1.0	-	-	500→630	15	2sp=poor	2sp=poor	350	3.76	11.7k	.86→1.8	n	41	6×10^{12}
18C	SI	none	1.0	-	-	400	30	2sp=poor	3sp-1n:ptof	400	3.39	5.1k	.73→1.11	n	108	3×10^{12}
18D	SI	none	1.0	100v	300μa	400	30	poortofair	9sp=good	400	3.61	4.7k	.82→1.13	n	19	2×10^{13}
19A	SI	none	1.0	100v	300μa	350°C	20	4sp=fair	very good	400	3.63	6.45k	.94 NL	n	84	3.8×10^{12}
19B	SI	none	1.0	100v	300μa	300°C	20	4sp=fair	poor	300	3.62	11.3k	1.0	n	686	4×10^{11}
19C	SI	none	1.0	75v	300μa	300	20	5sp=fair	8sp=good	500	3.59	7.88k	1.07	n	212	2.2×10^{12}
19D	SI	none	1.0	75v	1ma	300°C	20	3sp=poor	7sp=good	425	3.47	11.9k	.76→1.05	n	46	6.3×10^{12}
20A	SI	none	1.0	+75 60v	300μa	300°C	200ev	2sp=poor	3sp=poor	?	3.68	3.45k	1.25	n	224	2.6×10^{12}
20B	SI	none	1.0	75v	500μa	300°C	20	2sp=poor	fair	400	3.65	6.14k	1.21	n	139	1.6×10^{12}
20C	SI	none	1.0	75v	200μa	300°C	22	1sp=poor	fair	400	3.74	7.4k	1.23	n	35	9.4×10^{12}
20D	SI	none	1.0	75v	300μa	300°C	20	1sp=poor	fair	?	3.58					
21A	SI	none	2.0μm	75v	300μa	300°C	20	poor	poor	400	3.79	22.9k	1.65 NL	not measured		
21B	SI	100%Si	2.0	75v	300μa	350°C	20	3sp=poor	2sp=poor	400	3.62	1.84	.166	n	80	3.5×10^{16}
21C	SI	100%Mg	2.0	75v	300μa	350	20	3sp=poor	7sp=good	400	4.13	3.15k	1.42 NL	n	49	1.8×10^{13}
22A	SI	100%As	2.0	75v	300μa	350°C	20	6sp=good	2sp=poor	400	4.15	463	NL	not measured		
22B	SI	100%As+100%Si	2.0	75v	300	350	20	3sp=poor	2sp=poor	400	4.37	1.40	.132	n	90	4.4×10^{16}
22C	SI	100%As+100%Mg	2.0	75v	300	350	20	6sp=good	3sp=poor	400	4.43	28.0k	1.05	not measured		
23A	SI	10%Si	2.0	75	300	350	20	2sp=poor	2sp=poor	400	3.99					
23B	SI	1%Si	2.0	75	300	350	20	3sp=poor	2sp=poor	400	3.97	3.92k	.53→1.19	n	121	8.3×10^{12}
23C	SI	0.1%Si	2.0	75	300	350	20	6sp=good	2sp=poor	400	4.08					
24A	SI	10%Si	2.0	75	300	350	20	2sp=poor	2sp=poor	400	4.06	1.86k	1.36	n	27	5.8×10^{13}
24B	SI	0.1%Si	2.0	75	300	350	20	2sp=poor	2sp=poor	400	4.08	11.9k	.54→1.01	n	153	2.1×10^{12}
24C	SI	none	0.1	75	300	350	20	6sp=good	2sp=poor	400	4.07					
25A	none	made	defective heater													
25B	SI	100%Mg	2.0	100	300	350	5	2sp=poor	none	400	3.66	1.12	.03→.09	p	5.45	1×10^{18}
25C	SI	10%Mg	2.0	100	300	350	5	3sp=fair	none	400	4.00	1.04	.02	p	17.9	3.3×10^{17}
26A	SI	100%As+Si	2.0	100	300	350	5	5sp=good	3sp=fair	400°C	4.16	broke before measurement				
26B	SI	"	2.0	100	300	350	5	6sp=good	6sp=good	450°C	4.09	1.01	.13	n	154	3.6×10^{16}
26C	SI	"	2.0	100	300	350	5	4sp=fair	6sp=good	350°C	4.03	.94	.13	n	80	7.8×10^{16}

The electrical results for sets 17 through 20 were quite difficult to obtain because of the high resistance of the samples. The current used was often in the range of 10 to 100 nA. This often led to charging effects in the cable capacitances which was affected by any motion of persons nearby. These problems were most pronounced during Hall effect measurements and those figures in the table are the most suspect. In addition, there is no clear relation apparent between the RED quality and good electrical properties. For example, sample 19B exhibited a high mobility even though it had a poor RED pattern. Sample 18D had a good RED pattern and poor mobility. No reasons were found for these discrepancies but it was decided that it was more important to move on to making doped samples which would be easier to measure and of more importance. The next samples were made thicker as a consequence of the possibility that the thin layers were being depleted by surface states and the Cr doped substrate [9].

The measurement of sample 21B marked the first dramatic indication that good films may be fabricated by this technique: a room temperature resistivity of 1.84 ohm-cm and mobility of 80 cm^2/volt sec. Of the 17 samples in sets 21 through 26, 9 provided good data which indicate significant trends. These are listed separately in Table VI. These were chosen because the measurements were stable, and repeatable. Of the other 8 samples, 3 broke before measurement, 1 was made for Auger analysis and 4 were unstable.

There are a number of points of interest in Table VI. Silicon doping always led to n-type material and magnesium doping resulted in p-type samples. Set 25 yielded the first p-type Hall effect measurements. Previous to that there had only been the polarity of some of the Schottky diodes and a possible p-n junction to indicate that p-type material had actually been made. Also, all of the doped samples were of lower resistivity than the undoped sample,

TABLE VI

Resistivity and Hall Effect Data Summary

Sample #	Dopants	Reflec. Electron Diff		Deposition		Resistivity at 30°C	Activation Energy	Type	Mobility (cm^2/V-sec	Carrier Concent.
		Substrate	Film	Temp (°C)	Rate (Å/sec)	(Ω-cm)	(eV)			
21 A	none	poor	poor	400	3.79	22.9 k	1.65	-	-	-
21 B	100% Si	poor	poor	400	3.62	1.84	.166	n	80	3.5×10^{16}
22 B	100% Si+As	poor	poor	400	4.37	1.49	.132	n	90	4.4×10^{16}
23 B	1% Si	poor	poor	400	3.97	3.92 k	.53→1.19	n	121	8.3×10^{12}
24 B	0.1% Si	poor	poor	400	4.08	11.9 k	.54→1.01	n	153	2.1×10^{12}
25 B	100% Mg	poor	none	400	3.66	1.12	.03→.09	p	5.5	1×10^{18}
25 C	10% Mg	fair	none	400	4.00	1.04	.02	p	18	3.3×10^{17}
26 B	100% Si+As	good	good	450	4.09	1.01	.13	n	154	3.6×10^{16}
26 C	100% Si+As	fair	good	350	4.03	.94	.13	n	80	7.8×10^{16}

21A. This is a seemingly obvious result but some films reported earlier [10] did not exhibit this dependence.

By comparing the characteristics of samples 21B and 22B it is seen that co-sputtering of arsenic appears to increase the mobility and carrier concentration and decrease the activation energy and resistivity in silicon doped samples. Each effect can be interpreted as indicating better films. It was decided that co-sputtering of arsenic should be a standard procedure. However, Table V shows that excess arsenic was not of clear benefit for magnesium doped films, see samples 21C and 22C. Whether this is a trend or not has not yet been determined at this time.

An important dependence can be seen by comparing the mobility of samples 21B, 23B and 24B. The mobility clearly increases with decreasing doping. The drop in carrier concentration, and the resulting sharp increase in the resistivity may be due to disorder-induced trapping levels which are filled in 21B but not in 23B and 24B. This will be considered more in the next section. One important point which is not shown in Table VI is that the mobility of sample 22B was measured at 103°K and found to be 11 cm^2/volt sec, the carrier concentration was $2.5 \times 10^{14}/cm^3$ and the resistivity was 2244 ohms. While this measurement was not as stable as those at room temperature, it is believed to be indicative of the real situation. None of the measurements on other samples attempted at this temperature were stable enough to be reliable.

The hole mobility in samples 25B and 25C also exhibit the expected increase with decreased doping density. This hole mobility is also about one order of magnitude less than the electron mobility, as would be expected.

Finally, the beginnings of a new set of temperature variation runs are seen in 26B and 26C. This time the samples were of sufficient quality to

yield more reliable measurements. Also the co-sputtering of excess arsenic was used. This seems to have increased the optimum temperature of deposition since 26B which was deposited at 450°C is clearly better than 26C done at 350°C. Sample 26B yielded a higher mobility but a lower carrier density. Perhaps the structure is improved but the sticking coefficient for silicon is reduced at the higher temperature.

Electron Beam Induced Current (EBIC) measurements were attempted on a number of samples from sets 9 to 15. One substrate was measured in order to become familiar with the technique. The result was a diffusion length of 0.46 microns. There was only one sputtered film which gave sufficient signal strength to be interpreted. This was sample 11-1 which was a 100% Si doped and a diffusion length of 0.048 microns was found. This technique will be used again once the van der Pauw measurements have been used to find the optimum deposition conditions.

The Selected Area Diffraction technique has also been tried on several samples. Figure 23 is an SAD photograph of a polished substrate. A pattern is clearly evident. Sample 19A, which gave the best RED pattern, was used to in the study shown in Fig. 24, which is not as clear as Fig. 23. This technique will also be pursued as the quality of the films improve.

E. Analysis of Results (van dew Pauw)

The central features which need to be analyzed in this data are the mobility, the carrier concentration,and the activation energy. The mobility is analyzed by considering the various possible limiting mechanisms, such as lattice scattering, polar mode scattering, ionized impurity scattering, and grain boundary, or other lattice imperfection, scattering. The carrier concentration will depend on the density of intended dopant material added, the density of any unintended impurities, particularly those which cause

compensation energy levels, and the concentration of traps due to crystalline imperfections. The activation energy can be that of the intended dopant, or it may be characteristic of the compensation or trap levels, if they are present, or of the grain boundary potential. Clearly, there are many possible combinations, in fact this list does not include all of them.

Some physical insight must be used to consider the data and decide what is likely to be of the most importance. One of the quite consistent numbers is the carrier concentration in the 100% Si doped samples. These values are all in the mid $10^{16}/cm^3$ range. However, the capacitance measurements indicated a donor density of $N_d = 5.7 \times 10^{18}/cm^3$ for sample 11-1, which is also 100% Si doped. The reason for the difference is that Hall effect measurements determine the density of free carriers and the capacitance measurements determine the density of charge centers in the film [9]. The difference is due to the density of traps, assuming complete donor ionization, which is to be expected for silicon in GaAs. This is the key to understanding most of the data in Table VI, because it suggests the presence of a very high ionized impurity level, a very high concentration of defect induced electron trap energy levels in the energy band gap, and numerous grain boundary scattering centers.

The carrier concentration and activation energy can be explained by noting that the 100% Si samples are doped heavily enough to fill the mid-gap traps and still leave a substantial electron population in the conduction band. This results in a relatively low activation energy because the mid-gap traps are not involved. However, with lighter doped Si samples, the mid-gap traps are not filled so the conduction band electron population is kept low and the activation energy is characteristic of mid-gap traps. On the other hand,

the mid-gap traps would not be expected to affect the carrier concentration in the p-type material [11] and it can be seen that it is indeed much higher. In fact, the carrier concentration in the p-type material measured here is higher than that determined from the capacitance measurements on sample 12-3. This is very likely due to the differences in the preparation techniques, particularly the deposition temperature. Sample 12-3 was prepared at a higher temperature than 25B and the Mg sticking coefficient would be expected to be less.

The limited mobility can be explained by the combination of ionized impurity scattering and grain boundary scattering. The Brooks-Herring equation for the mobility expected from ionized impurity scattering is [12]:

$$\mu_I = \frac{3.28 \times 10^{15} \cdot \varepsilon_r^2 T^{3/2}}{m^{*1/2}(2N_A+n)\{\ln(b+1)-[b/(b+1)]\}} , \quad (cm^2/V\text{-sec.}) \qquad (15)$$

where

$$b = \frac{1.29 \times 10^{14} m^* \varepsilon T^2}{n^*} , \qquad (16)$$

and

$$n^* = n + [(n + N_A)(N_D - N_A - n)/N_D] \ (cm^{-3}) . \qquad (17)$$

The 100% Si doped case will be considered. It is assumed that all of the donors are ionized. This results in $n = N_D - N_A$ or $N_A = N_D - n$, where N_A is here the trap density. As a result, $n^* = n$. In this case, $b = 257$ and $\mu_I = 213\ cm^2/V$ sec. Clearly, the very high doping impurity levels will severely limit the mobility.

According to Anderson [13], the mobility limitation for polycrystalline samples due to grain boundary scattering can be written as:

$$\mu_B = \frac{q\langle c\rangle d}{kT} , \qquad (18)$$

where $\langle c\rangle$ is the average thermal velocity, d is the average crystallite

size and q, k,T have their usual meanings. The problem here is in determining d. An estimate could be made from N_A. It is unknown how many traps to ascribe to each grain, but as a first approximation it seems reasonable to say one for each direction along each of three dimensions for a total of six per grain. This gives,

$$d = \left(\frac{N_a}{6}\right)^{-1/3} = 1.02 \times 10^{-6} \text{ cm} . \tag{19}$$

The average thermal velocity is about $\langle c \rangle \simeq 3.66 \times 10^7$ cm/sec.

In this case, $\mu_B \simeq 1443$ cm^2/V sec. The effect of these two mechanisms can be combined by calculating

$$\mu = \left[\frac{1}{\mu_I} + \frac{1}{\mu_B}\right]^{-1}$$

$$= 186 \text{ cm}^2/\text{volt sec} . \tag{20}$$

Considering the uncertainties involved in this calculation, this is quite close to the observed values. It should also be noted that the one low temperature mobility measured was compatible with the hypothesis of the importance of ionized impurity scattering.

It is therefore concluded that the above analysis is close to the actual case in these films. It is clear, without calculations, that the trend of the mobility with change in doping level is correct. Also, as was mentioned before, the relative electron and hole mobilities are as expected for GaAs.

IV. CONCLUSIONS

A large number of sputtered GaAs films have been fabricated and studied. These studies have consisted of two types, Schottky barrier measurements and van der Pauw measurements.

It was discovered early in these tests that the Schottky barrier electrical characteristics did not match those of the simple theory, nor any others reported

in the literature. This discovery led to a series of measurements in an attempt to determine the film properties from the properties of the Schottky barriers measured. A measure of the magnitude and phase angle of the device impedance as a function of frequency and temperature led to a circuit model description of the device. An analysis of this data combined with the capacitance-voltage data allowed the determination of the numerical values of the circuit elements in the model. These elements were, in turn, related to the physical parameters of the GaAs films and contacts. These results then led to a determination of the metal-semiconductor barrier height, "bulk" activation energy, conductivity, and doping concentration. This analysis is not yet completed.

A considerable amount of progress has been made in the quality of the films produced during this period. The electron and hole mobilities measured using the van der Pauw technique have advanced several orders of magnitude. Although improvement is still necessary, the approach to be used to develop high quality GaAs films deposited by sputtering has been identified. This work is continuing.

APPENDIX A

Circuit Analysis of Two Parallel RC Circuits in Series

The circuit to be analyzed consists of R_{SB} and C_{SB} in parallel and this circuit is in series with the parallel combination of R_B and C_B as shown in Fig. 11. R_{SH} is assumed to be zero. The complex impedance of such a circuit is given by:

$$Z = \frac{R_{SB}}{1+j\omega R_{SB}C_{SB}} + \frac{R_B}{1+j\omega R_B C_B} \quad , \tag{A-1}$$

where $j = \sqrt{-1}$ and $\omega = 2\pi f$, and f is the frequency. This complex impedance cannot be measured directly, but the magnitude and phase angle can be measured [5]. The magnitude of the impedance is given by,

$$|Z| = R_S \left[\frac{1+\omega^2 R_p^2 C_p^2}{(1+\omega^2 R_{SB}^2 C_{SB}^2)(1+\omega^2 R_B^2 C_B^2)} \right]^{1/2} , \tag{A-2}$$

and the phase angle by,

$$\theta = \tan^{-1}\omega R_P C_P - \tan^{-1}\omega R_{SB}C_{SB} - \tan^{-1}\omega R_B C_B \quad . \tag{A-3}$$

In these equations

$$R_S = R_{SB} + R_B \ , \tag{A-4}$$

$$R_P = R_{SB}R_B/R_S \ , \text{ and} \tag{A-5}$$

$$C_P = C_{SB} + C_B \ . \tag{A-6}$$

The time constants in eqn. (A-3) are identified as $T_{SB} = R_{SB}C_{SB}$, $T_B = R_B C_B$, and $T_P = R_P C_P$. Another time constant T_S is identified as $T_S = R_S C_S$ where,

$$C_S = C_{SB}C_B/C_P \quad . \tag{A-7}$$

It can be seen that

$$T_S T_P = T_{SB} T_B \quad . \tag{A-8}$$

If one of the time constants T_{SB} or T_B is much larger than the other, e.g. if $T_{SB} > > T_B$, then

$$T_B < < T_P < < T_{SB} \quad . \tag{A-9}$$

In this case, for low frequencies

$$\theta_L \simeq - \tan^{-1} \omega R_{SB} C_{SB} \quad , \tag{A-10}$$

the phase angle will be negative and decreasing with frequency. At intermediate frequencies,

$$\theta_I \simeq - \tan^{-1} \omega R_{SB} C_{SB} + \tan^{-1} \omega R_P C_P \quad , \tag{A-11}$$

and the phase angle will be negative but increasing. Finally, at high frequencies θ will be given by eqn. (A-3) and will be negative and decreasing again. The resulting plot of θ vs f will show a relative minimum and, at a higher frequency, a relative maximum, and then monotonically decrease with increasing frequency.

APPENDIX B

Capacitance-Voltage Characteristics of Thin-Film Schottky Barrier Diodes

A Schottky barrier formed on a thin layer of n-type GaAs which is deposited onto an n^+ GaAs substrate has an equilibrium energy band diagram as shown in Fig. 11, which includes the equivalent circuit model for such a structure. In order to determine the effective capacitance of this device solutions to Poisson's equation must be made in regions I, $0 \leq x \leq w_1$, and II, $w_2 \leq x \leq w_3$. Under conditions when the Schottky barrier is reverse biased the n^+n junction is "forward" biased. According to Jonscher [14] the quasi-Fermi level undergoes an abrupt change in slope at the metallurgical n^+n junction with a constant slope on eigher side of the junction. By current continuity considerations $\mathcal{E}_L\sigma_L = \mathcal{E}_H\sigma_H$, where $\mathcal{E}$ is the electric field and σ the conductivity, the sub L refers to the lightly doped n-type material and the sub H to the heavily doped n^+-type material. Since $\sigma_H >> \sigma_L$ the electric fields are such that $\mathcal{E}_H << \mathcal{E}_L$. In this case the portion of the applied voltage dropped across the n^+n depletion region, $w_3 \leq x \leq w_4$, is negligible and this region can be ignored.

The exact problem is very difficult to solve as a consequence of the non-uniform distribution of the accumulated charge in region II. However, a very good approximation can be made by assuming a uniform accumulation of charge in region II and a uniform depletion of electrons in region I.

The equations to be solved are:

$$\frac{d^2\psi_1}{dx^2} = \frac{-qN_{d1}}{\varepsilon_r\varepsilon_o} \tag{B-1}$$

in region I and

$$\frac{d^2 \psi_2}{dx^2} = \frac{q \Delta n}{\varepsilon_r \varepsilon_o} \qquad \text{(B-2)}$$

in region II. In these expressions ε_r is the relative dielectric constant, ε_o is the permittivity of free space, q is the electronic charge, N_{d1} is the donor concentration in the n-type film, n is the excess electron concentration in region II, and ψ is the electrostatic potential.

The boundary conditions necessary to solve eqn. (B-1) are:

$$\psi_1(w_1) = V_j - (V_a - V_b - V_{aLH}) \qquad \text{(B-3)}$$

and

$$\left.\frac{d\psi_1}{dx}\right|_{x=w_1} = - \frac{V_b}{w_2 - w_1} \quad , \qquad \text{(B-4)}$$

where V_j is the Schottky barrier built-in potential, V_a is the applied bias, V_b is that portion of the applied bias dropped across the "bulk" of the thin film, and V_{aLH} is the portion of V_a dropped at the low-high junction. The necessary boundary conditions for eqn. (B-2) are:

$$\psi_2(w_2) = V_j - (V_a - V_{aLH}) \qquad \text{(B-5)}$$

and

$$\left.\frac{d\psi_2}{dx}\right|_{x=w_2} = - \frac{V_b}{w_2 - w_1} \quad . \qquad \text{(B-6)}$$

The solution to eqn. (B-1) using (B-3) and (B-4) is:

$$\psi_1(x) = V_j - V_a + V_{aLH} + \frac{V_b(w_2 - x)}{w_2 - w_1} - \frac{qN_{d1}}{2\varepsilon_r \varepsilon_o} (x - w_1)^2 \quad , \qquad \text{(B-7)}$$

and the solution to eqn. (B-2) using (B-5) and (B-6) is

$$\psi_2(x) = V_j - V_a + V_{aLH} + \frac{V_b(w_2 - x)}{w_2 - w_1} + \frac{q\Delta n}{2\varepsilon_r \varepsilon_o} (x - w_2)^2 \quad . \qquad \text{(B-8)}$$

Additional conditions are necessary in order to determine the space-charge region widths, w_1 and w_3-w_2. These conditions are

$$\psi_1(o) = 0 \tag{B-9}$$

and

$$\psi_2(w_3) = V_j + V_{LH} - V_a \quad , \tag{B-10}$$

where V_{LH} is the n^+n junction built-in potential assuming all the potential is dropped in region II. A substitution of eqn. (B-9) into eqn. (B-7) yields an expression which can be solved for w_1,

$$\psi_1(o) = V_j - V_a + V_{aLH} + \frac{V_b w_2}{w_2 - w_1} - \frac{qN_{d1}w_1^2}{2\varepsilon_r\varepsilon_o} = 0 \quad . \tag{B-11}$$

This is a cubic equation in w_1, however

$$V_b = R_B I, \tag{B-12}$$

where R_B is the film resistance and I is the current flowing. Under reverse bias conditions $I = -I_o$, the reverse bias leakage current, assumed constant, and

$$R_B = \frac{w_2 - w_1}{\sigma_L A} = \frac{w_2 - w_1}{q\mu_n N_{d1} A} \quad , \tag{B-13}$$

where A is the device area. Solving eqn. (B-11) for w_1 using eqns. (B-12) and (B-13) yields

$$w_1 = \left[\frac{2\varepsilon_r\varepsilon_o}{qN_{d1}} \left(V_j - V_a + V_{aLH} - \frac{I_o w_2}{q\mu_n N_{d1} A} \right) \right]^{1/2} . \tag{B-14}$$

The capacitance of region I, C_{SB}, is given by

$$C_{SB} = \left| \frac{dQ_1}{dV_a} \right| \quad , \tag{B-15}$$

where

$$Q_1 = qN_{d1}Aw_1 \quad . \tag{B-16}$$

The resulting expression for C_{SB} is:

$$C_{SB} = \frac{\varepsilon_r \varepsilon_o A}{\left[\frac{2\varepsilon_r \varepsilon_o}{qN_{d1}} (V_j - V_a + V_{aLH} - \frac{I_o w_2}{q\mu_n N_{d1} A})\right]^{1/2}} = \frac{\varepsilon_r \varepsilon_o A}{w_1} \quad . \quad \text{(B-17)}$$

It can be seen that if R_B is small and V_{aLH} is small this reduces to the expression for a normal Schottky barrier diode:

$$C = A \left[\frac{qN_{d1}\varepsilon_r \varepsilon_o}{2(V_j - V_a)}\right]^{1/2} \quad . \quad \text{(B-18)}$$

Substitution of eqn. (B-10) into eqn. (B-9) using eqns. (B-12) and (B-13) again yields an expression which can be solved for $w_3 - w_2$,

$$\frac{q\Delta n}{2\varepsilon_r \varepsilon_o} (w_3 - w_2)^2 + \frac{I_o (w_3 - w_2)}{q\mu_n N_{d1} A} + V_{aLH} - V_{LH} = 0 \quad . \quad \text{(B-19)}$$

The solution to eqn. (B-19) is:

$$w_3 - w_2 = \frac{I_o \varepsilon_r \varepsilon_o}{q^2 \mu_n N_{d1} \Delta n A} \left\{\left[1 + \frac{2(V_{LH} - V_{aLH}) q^3 \mu_n^2 N_{d1}^2 \Delta n A^2}{\varepsilon_r \varepsilon_o I_o^2}\right]^{1/2} - 1\right\} \quad \text{(B-20)}$$

.

For any reasonable values

$$\frac{2(V_{LH} - V_{aLH}) q^3 \mu_n^2 N_{d1}^2 \Delta n A^2}{\varepsilon_r \varepsilon_o I_o^2} >> 1 \, , \quad \text{(B-21)}$$

with the result that

$$w_3 - w_2 \approx \left[\frac{2\varepsilon_r \varepsilon_o (V_{LH} - V_{aLH})}{q\Delta n}\right]^{1/2} \quad . \quad \text{(B-22)}$$

The resulting capacitance of the high-low junction is

$$C_{LH} = \left|\frac{dQ_2}{dV_a}\right| = \left|\frac{dQ_2}{dV_{aLH}}\right| \left|\frac{dV_{aLH}}{dV_a}\right|$$

$$= A \left[\frac{2\varepsilon_r \varepsilon_o q\Delta n}{(V_{LH} - V_{aLH})}\right]^{1/2} \frac{dV_{aLH}}{dV_a} \quad . \quad \text{B-23)}$$

An additional capacitance remains to be evaluated and it is that of the thin film GaAs dielectric. This capacitance is given by

$$C_B = \frac{\varepsilon_r \varepsilon_o A}{w_2 - w_1} \quad . \tag{B-24}$$

The equivalent circuit of the device is that of three parallel RC circuits in series, as shown in Fig. 11. R_{SB} is the ac small signal resistance of the Schottky barrier, $R_{SB} = dV_a/dI$, R_B is the resistance of the film neutral region and is given in eqn. (B-13), and R_{LH} is the ac resistance of the n^+n junction. According to Jonscher [14] the resistance of the n^+n junction under forward bias is very small and will effectively short out this junction capacitance, C_{LH}. The result is a circuit model which consists of two RC parallel circuits in series. This model has been discussed elsewhere [5] but not when considering the bias voltage dependence of capacitance.

A capacitance bridge will measure the equivalent parallel capacitance which is given by

$$C_{par} = \frac{R_{SB}^2 C_{SB} + R_B^2 C_B + \omega^2 R_{SB}^2 R_B^2 C_{SB} C_B (C_{SB} + C_B)}{(R_{SB} + R_B)^2 + \omega^2 R_{SB}^2 R_B^2 (C_{SB} + C_B)^2} \quad . \tag{B-25}$$

At high frequencies this expression reduces to the capacitance of two series capacitances:

$$C_{par\infty} = \frac{C_{SB} C_B}{C_{SB} + C_B} \quad . \tag{B-26}$$

This capacitance can be evaluated as a function of applied bias using eqns. (B-17), (B-24), and (B-14). The resulting expression is:

$$C_{par\infty} = \frac{\left(\frac{A\varepsilon_r\varepsilon_o}{w_1}\right)\left(\frac{A\varepsilon_r\varepsilon_o}{w_2 - w_1}\right)}{\frac{A\varepsilon_r\varepsilon_o}{w_1} + \frac{A\varepsilon_r\varepsilon_o}{w_2 - w_1}} = \frac{A\varepsilon_r\varepsilon_o}{w_2} \quad . \tag{B-27}$$

It can be seen that this capacitance is just that of the thin film dielectric if there is no depletion layer and is independent of applied bias, V_a.

At very low frequencies the equivalent parallel capacitance reduces to

$$C_{pardc} = \frac{R_{SB}^2 C_{SB} + R_B^2 C_B}{(R_{SB} + R_B)^2} \quad . \tag{B-28}$$

Since all terms in eqn. (B-28) vary with applied voltage in differing manners, it becomes very difficult to determine the properties of the films from C-V measurements. Of course, the intermediate frequency expression, eqn. (B-25) is even more complicated. For this reason an analysis of the device properties was made using complex impedance versus frequency measurements to determine R_{SB}, C_{SB}, R_B, and C_B for this circuit model.

APPENDIX C

Computer Program to Determine Component Values of Circuit Elements in Fig. 11

```
SIGNATURE*MODEL(1), GAAS
     1      C
     2      C ..... PROGRAM TO COMPUTER OPTIMUM CIRCUIT PARAMETERS.....
     3      C ..... FOR CIRCUIT MODEL OF THIN FILM GA-AS JUNCTION .....
     4      C
     5            DIMENSION  THETA(12), FREQ(12)
     6            DATA FREQ/100.0,200.0,500.0,1000.0,2000.0,5000.0,
     7           >10000.0,20000.0,50000.0,100000.0,200000.0,500000.0,
     8      C
     9      C
    10            DO 1 N = 1,12
    11      1     READ *,THETA(N)
    12      C
    13            NDXMIN = 1
    14            RMSMIN = 1000000.0
    15            TWOPI = 2.0*3.14159
    16            READ *,A,T1
    17            READ *,FLOW,FHIGH
    18            STEP = (FHIGH-FLOW)/1000
    19      C
    20            DO 2 N = 1,1000
    21            T2 = FLOW + FLOAT(N)*(STEP)
    22            RMS = 0.0
    23      C
    24            DO 3 M = 1.12
    25            OMEGA = FREQ(M)*TWOPI
    26            THETAC = ATAN(OMEGA*A*T2) - ATAN(OMEGA*T1)
    27           >        -ATAN(OMEGA*T2)
    28            THETAC = THETAC*57.2
    29            RMS = RMS + (THETA(M) - THETAC)**2
    30      3     CONTINUE
    31      C
    32            IF (RMS.LT.RMSMIN) THEN
    33               NDXMIN = N
    34               RMSMIN = RMS
    35            END IF
    36      2     CONTINUE
    37      C
    38            T2 = FLOW + FLOAD(NDXMIN)*(STEP)
    39            PRINT *,'OPTIMUM T2 = ',T2
    40            RMSMIN = SQRT(RMSMIN/12.0)
    41            PRINT *,'RMS ERROR = ',RMSMIN
    42      C
    43            PRINT *,'VALUES OF THETA.....'
    44      C
    45            DO 4 I = 1,12
    46            OMEGA = FREQ(I)*TWOPI
    47            THETAC = ATAN(OMEGA*A*T2) - ATAN(OMEGA*T1)
    48           >        -ATAN(OMEGA*T2)
    49            THETAC = THETAC*57.2
    50            PRINT *,THETAC
    51      4     CONTINUE
    52            STOP
    53            END
```

REFERENCES

1. J. R. Arthur, Perkin-Elmer, Physical Electronics, private communication.
2. L. J. van der Pauw, "A Method of Measuring Specific Resistivity and Hall Effect of Disks of Arbitrary Shape", Philips Research Reports 13, 1 (1958).
3. R. J. Soukup, "Gallium Arsenide Films Sputter Deposited onto Gallium Arsenide Substrates", Annual Report, Grant No. AFOSR-77-3155, University of Nebraska, Lincoln, Nebraska, 1 October 1976-30 September 1977.
4. M. P. Healy and R. J. Mattauch, "Low Temperature Ohmic Contacts to Gallium Arsenide Using In and Al", IEEE Trans. Electron Dev. ED-23, 374 (1976).
5. R. J. Soukup, D. M. Mosher, and A. K. Kulkarni, "The Through Film Electrical Properties of Sputtered GaAs Films With Aluminum Contacts", Thin Solid Films 52, 237 (1978).
6. L. J. van der Pauw, "A Method of Measuring the Resistivity and Hall Coefficient on Lamellae of Arbitrary Shape", Philips Tech. Rev. 20, 220 (1958/9).
7. Jim-Yong Chi and Harry C. Gatos, "Non-Destructive Determination of the Depth of Planar pn Junctions by Scanning Electron Microscopy", IEEE Trans. El. Dev. ED-24, 1366 (1977).
8. G. R. Booker, A.M.B. Shaw, M.J. Whelan, and P.B. Hirsch, "Some Comments on the Interpretation of the 'Kikuchi-like Reflection Patterns' observed by Scanning Electron Microscopy", Phil. Mag. 16, 1185 (1967).
9. P. L. Hower, W. W. Hooper, B.R. Cairns, R. D. Fairman, and D. A. Tremere, "The GaAs Field-Effect Transistor", Semiconductors and Semimetals, Ed. R. K. Willardson and A. C. Beer, Vol. 7, Part A, Academic Press, New York and London, pp. 147-202 (1971).
10. R. J. Soukup, "The Electrical Properties of Sputtered Gallium Arsenide Films", Final Report, Grant No. AFOSR 76-2941, University of Iowa, Iowa City, Iowa, 1 November 1975-31 August 1976.

11. F. J. Blatt, Physics of Electronic Conduction in Solids, McGraw Hill, New York, 1968, p. 180.

12. C. M. Wolfe, G. E. Stillman, and J. O. Dimmock, "Ionized Impurity Density in n-type GaAs", J. Appl. Phys. 41, 504 (1970).

13. J. C. Anderson, "Barrier-Limited Mobility in Thin Semiconducting Films", Thin Solid Films 18, 239 (1973).

14. A. K. Jonscher, Principles of Semiconductor Device Operation, G. Bell & Sons, Ltd., London, (1960) pp. 142-144.

LIST OF FIGURES

Page

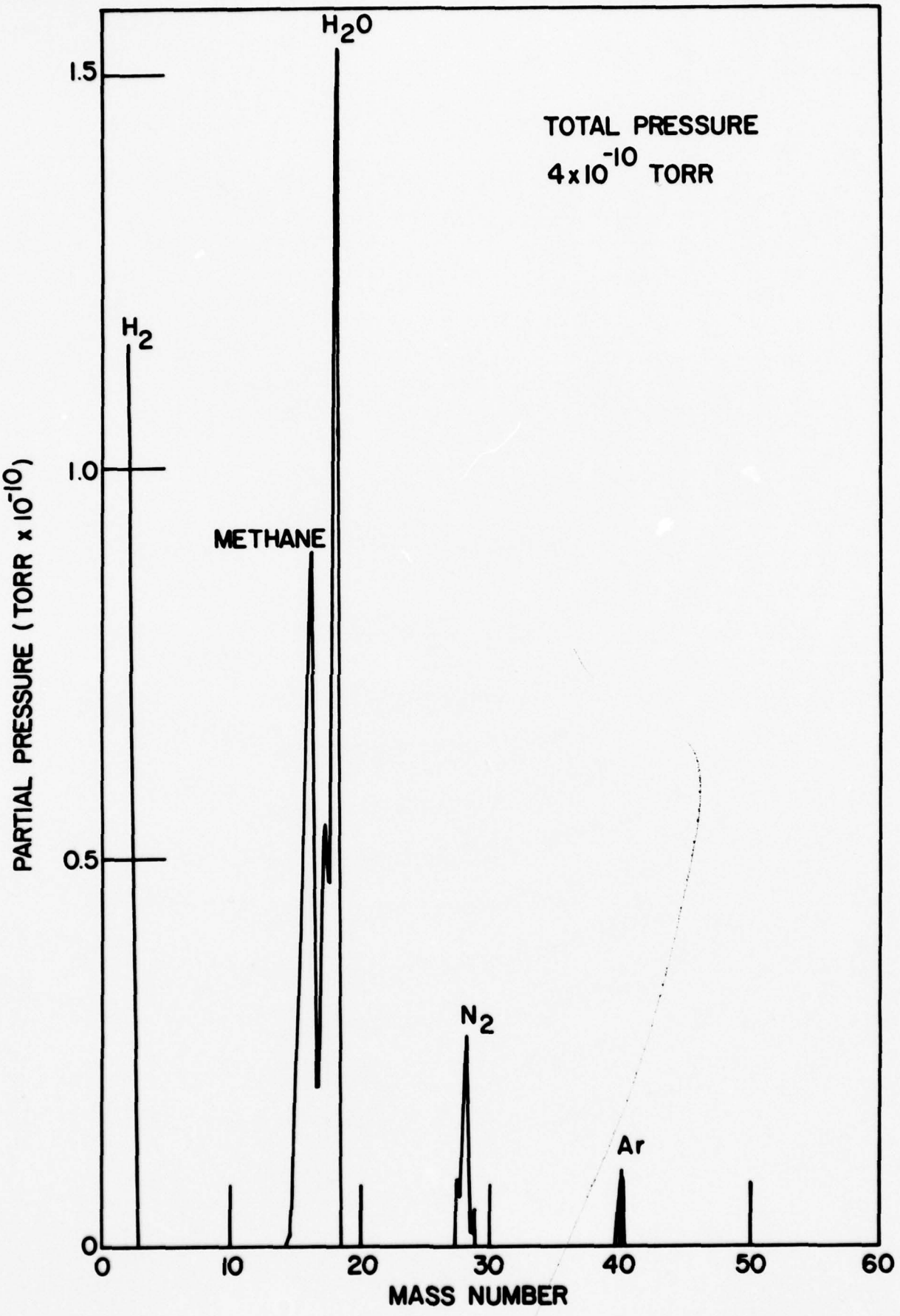
H2O
1.5
TOTAL PRESSURE
4x10^-10 TORR
H2
1.0
METHANE
PARTIAL PRESSURE (TORR x 10^-10)
0.5
N2
Ar
0
0
10
20
30
40
50
60
MASS NUMBER

Figure 1

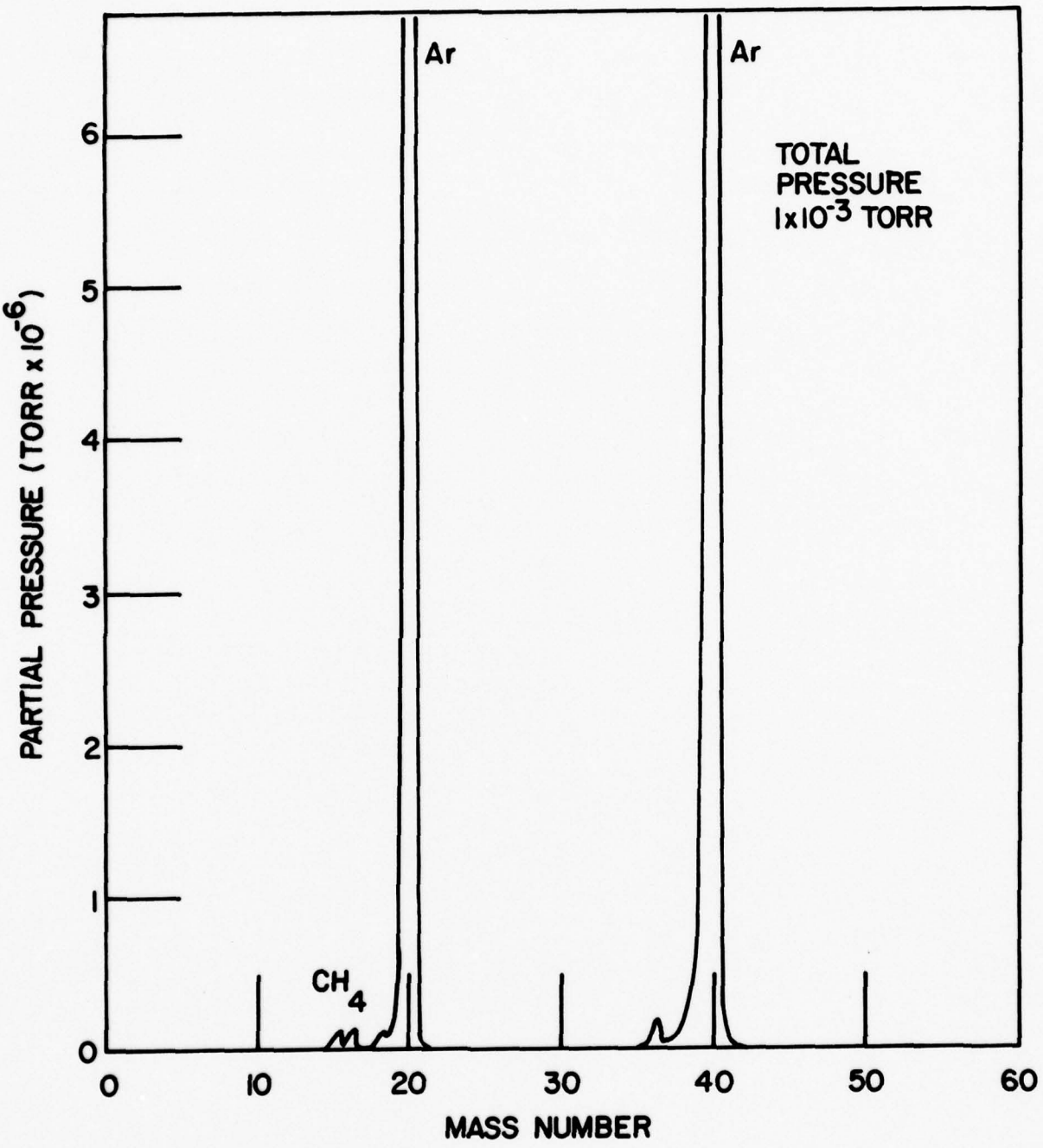
Ar
Ar
TOTAL
PRESSURE
1x10-3 TORR
CH4
PARTIAL PRESSURE (TORR x 10-6)
0
1
2
3
4
5
6
0
10
20
30
40
50
60
MASS NUMBER

Figure 2

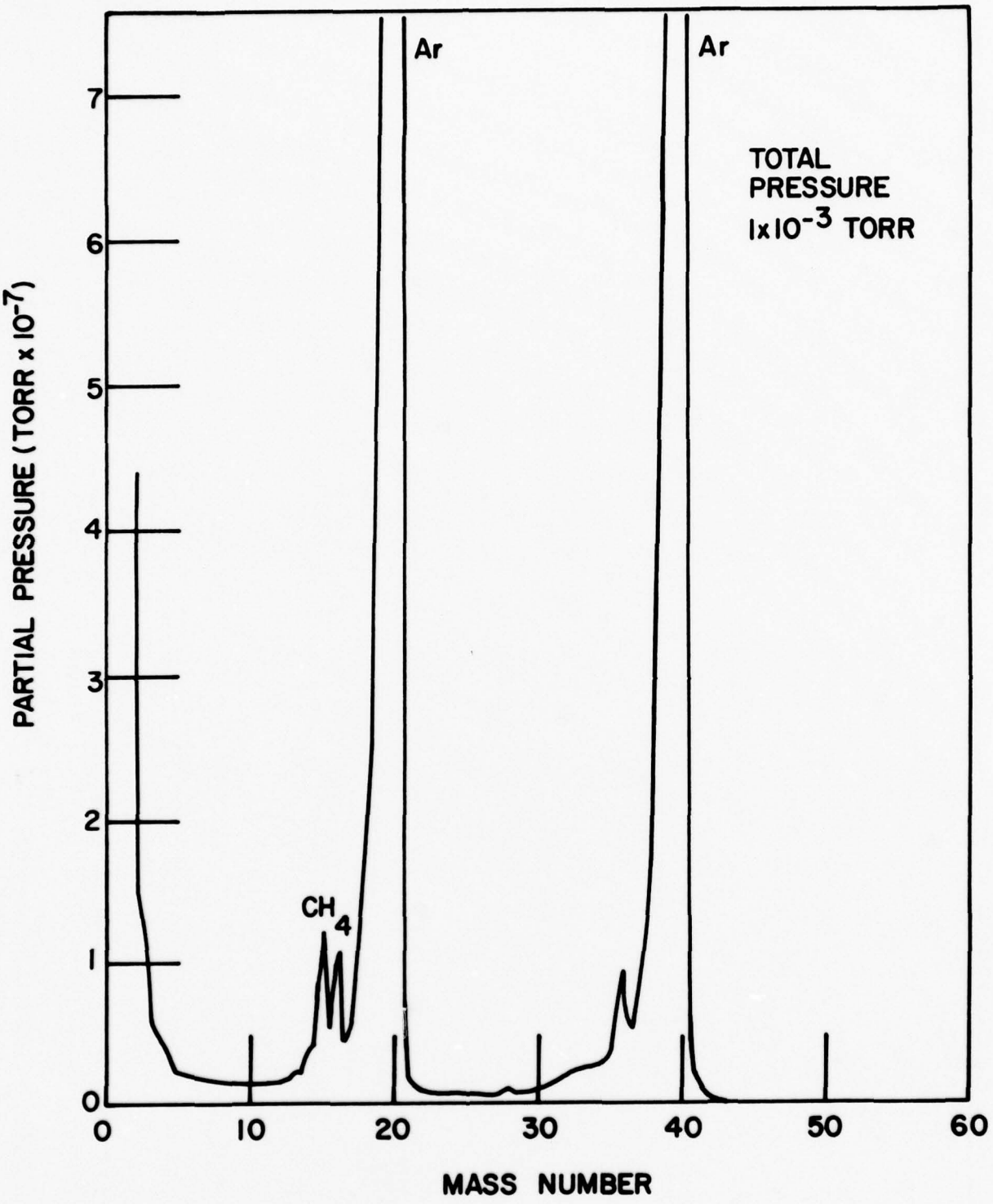
Ar
Ar
TOTAL
PRESSURE
1x10-3 TORR
CH4
PARTIAL PRESSURE (TORR x 10-7)
0
1
2
3
4
5
6
7
0
10
20
30
40
50
60
MASS NUMBER

Figure 3

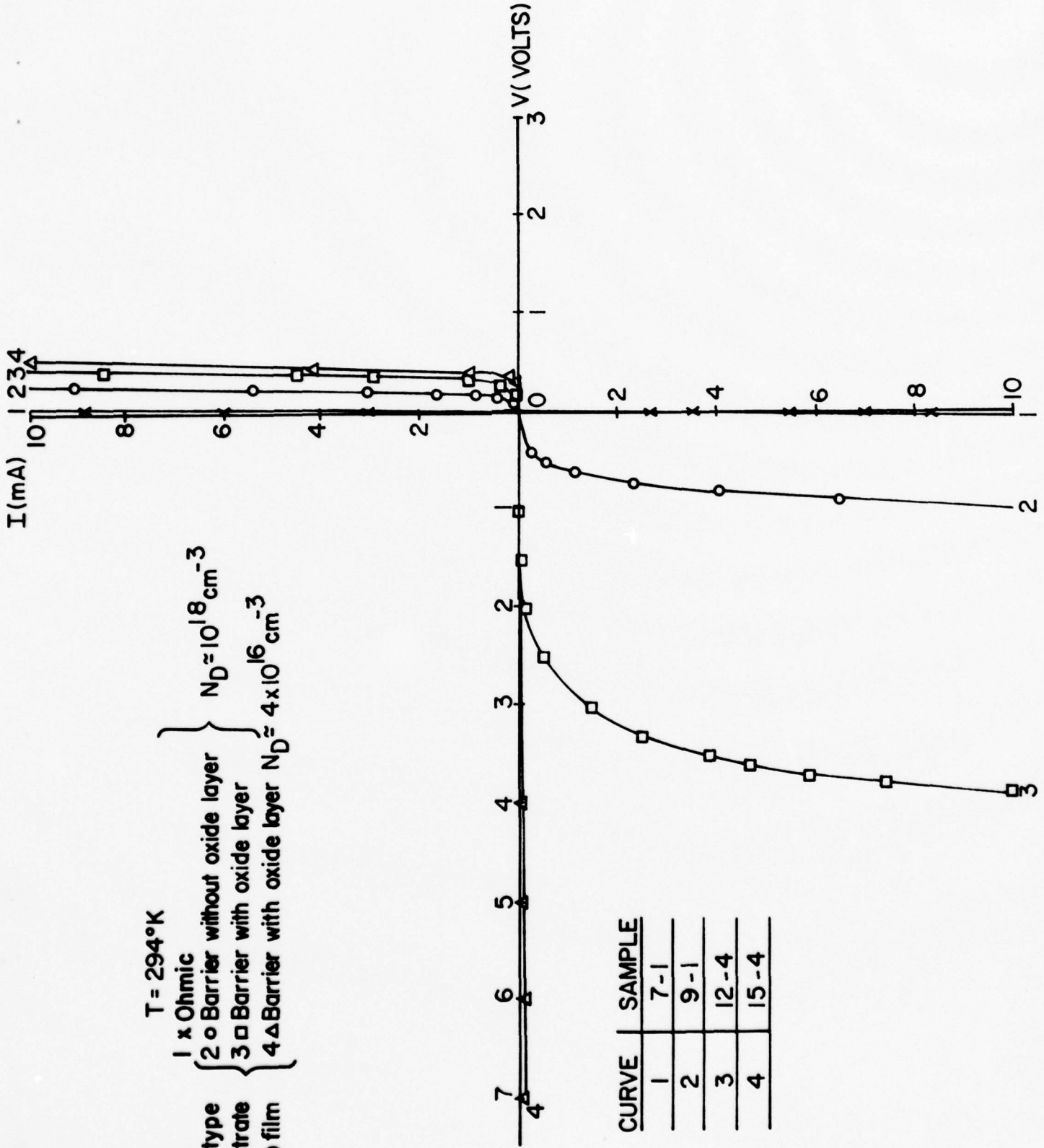
I(mA)
V(VOLTS)
T= 294°K
1 x Ohmic
2 o Barrier without oxide layer
3 □ Barrier with oxide layer
4 △ Barrier with oxide layer
n-type substrate no film
$N_D \cong 10^{18} cm^{-3}$
$N_D \cong 4 \times 10^{16} cm^{-3}$
CURVE | SAMPLE
1 | 7-1
2 | 9-1
3 | 12-4
4 | 15-4

Figure 4

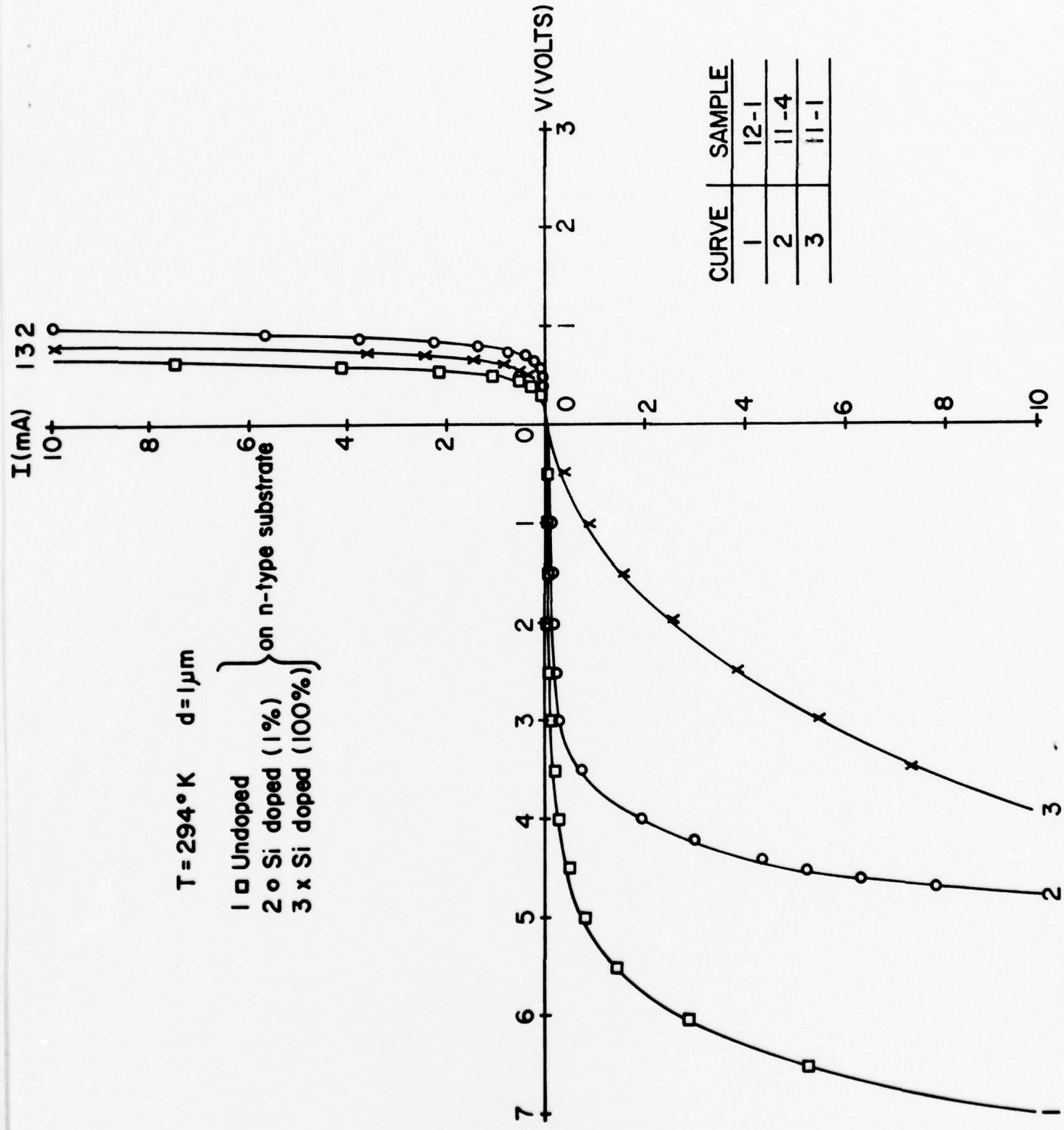
I(mA)
10
8
6
4
2
0
2
4
6
8
10
V(VOLTS)
0
1
2
3
4
5
6
7
T=294°K d=1μm
1 □ Undoped
2 ○ Si doped (1%)
3 x Si doped (100%)
on n-type substrate
CURVE | SAMPLE
1 | 12-1
2 | 11-4
3 | 11-1

Figure 5

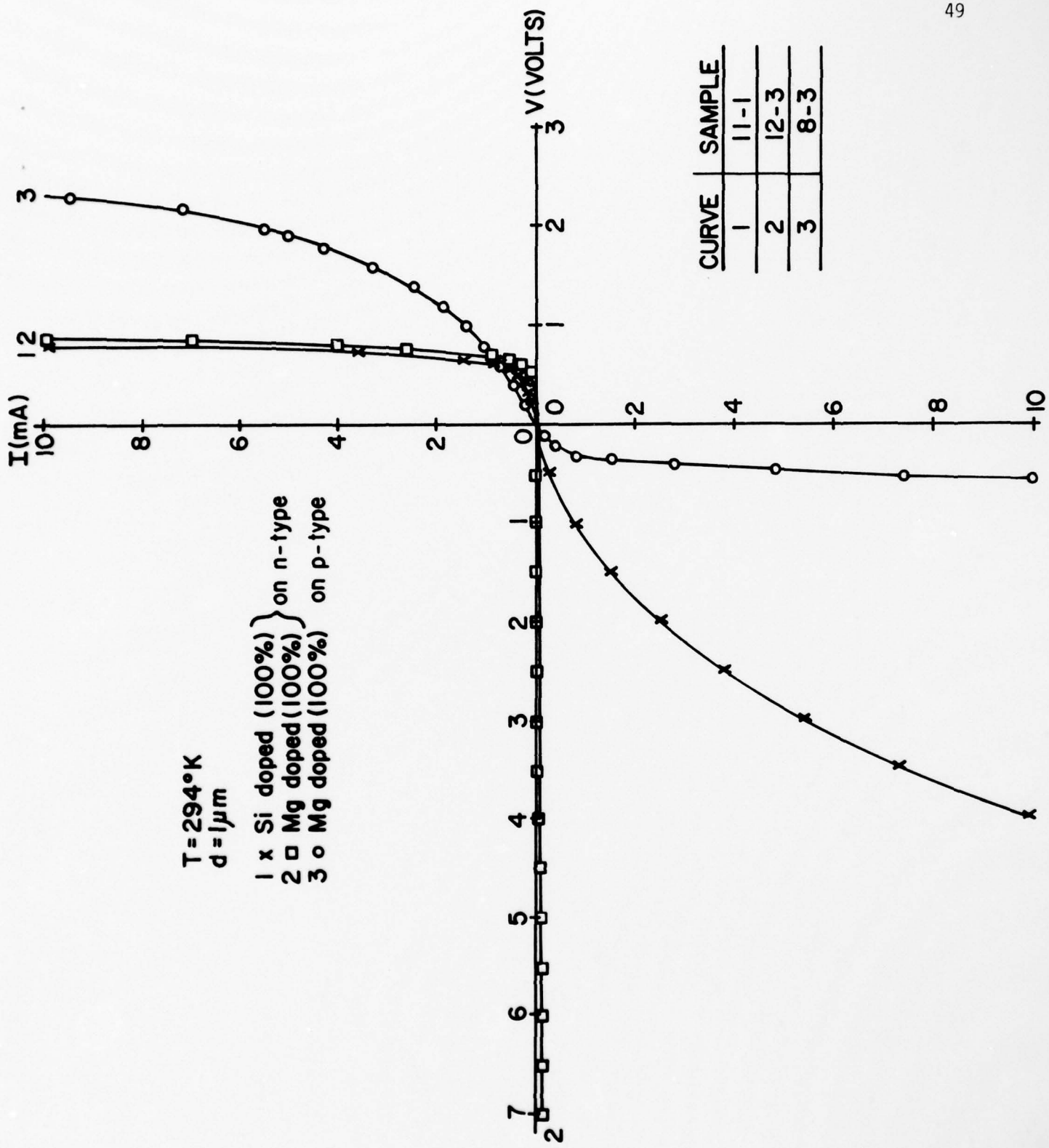
I(mA)
V(VOLTS)
T=294°K
d=1μm
1 x Si doped (100%) } on n-type
2 □ Mg doped (100%) }
3 o Mg doped (100%) on p-type
CURVE | SAMPLE
1 | 11-1
2 | 12-3
3 | 8-3

Figure 6

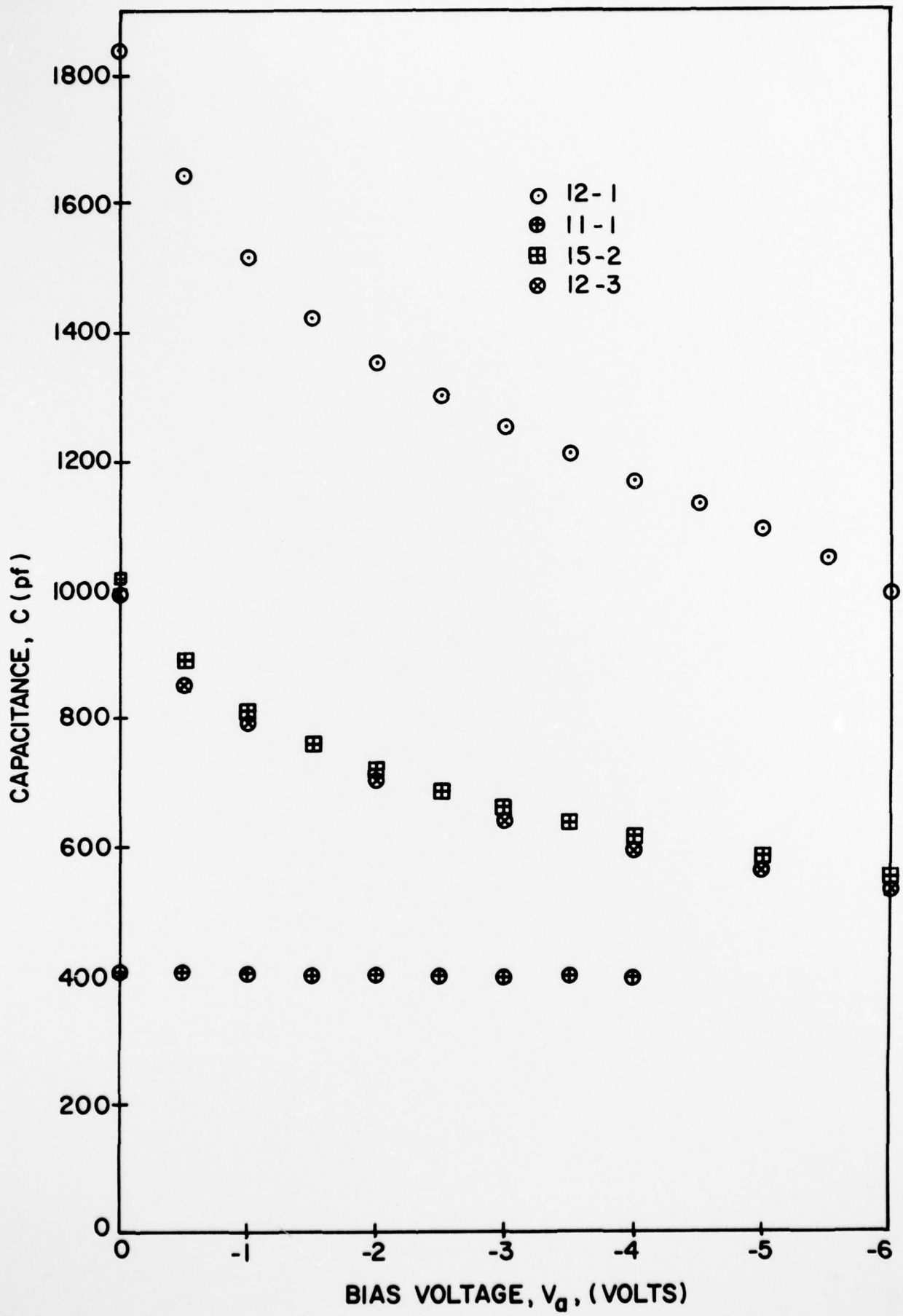
1800
1600
1400
1200
1000
800
600
400
200
0
CAPACITANCE, C (pf)
12-1
11-1
15-2
12-3
0
-1
-2
-3
-4
-5
-6
BIAS VOLTAGE, V_a, (VOLTS)

Figure 7

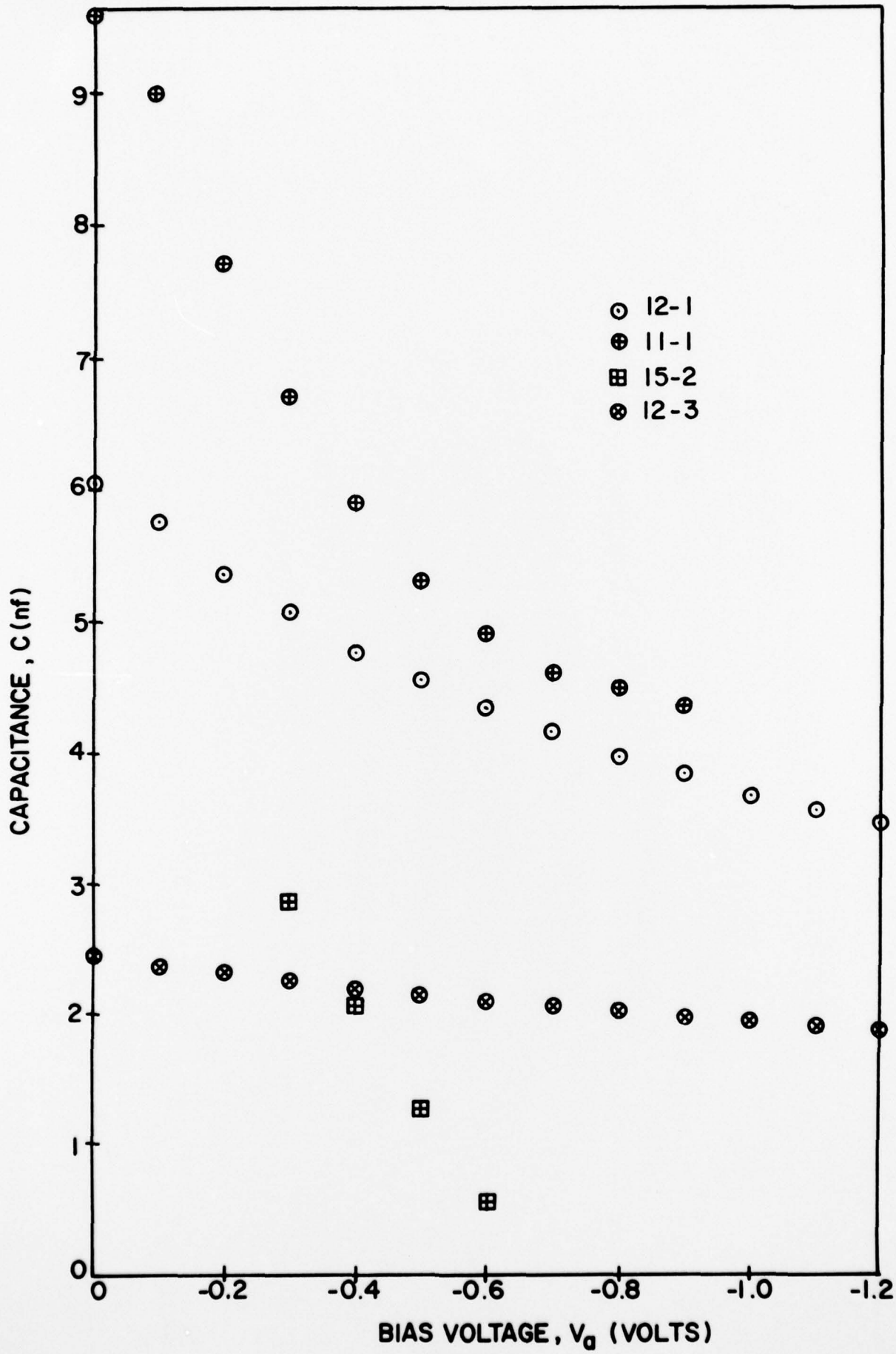
12-1
11-1
15-2
12-3
CAPACITANCE, C (nf)
BIAS VOLTAGE, V_a (VOLTS)
0
1
2
3
4
5
6
7
8
9
0
-0.2
-0.4
-0.6
-0.8
-1.0
-1.2

Figure 8

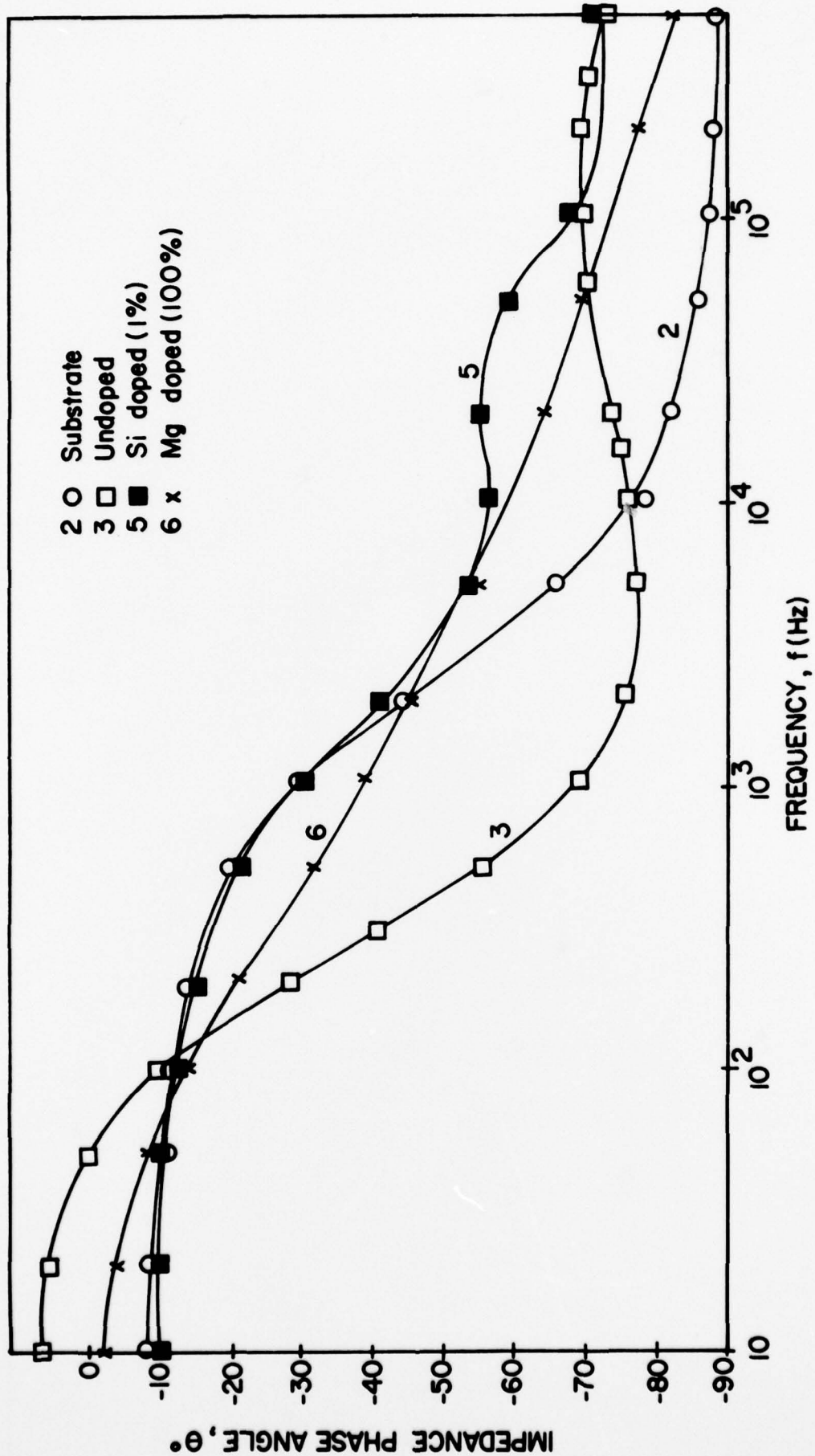
2 O Substrate
3 □ Undoped
5 ■ Si doped (1%)
6 x Mg doped (100%)
IMPEDANCE PHASE ANGLE, θ°
0
-10
-20
-30
-40
-50
-60
-70
-80
-90
10
10^2
10^3
10^4
10^5
FREQUENCY, f (Hz)
2
3
5
6

Figure 9

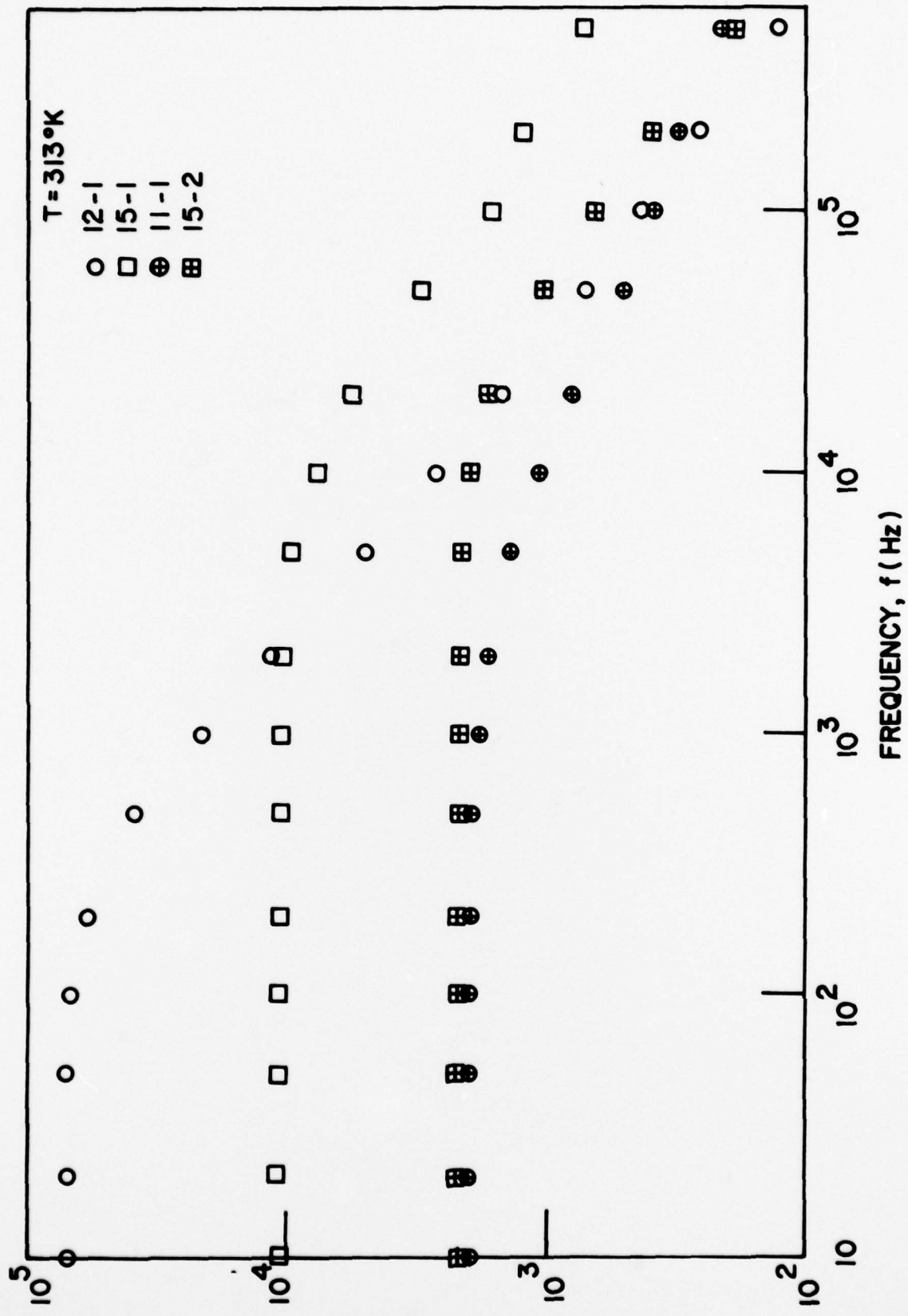
T=313°K
12-1
15-1
11-1
15-2
IMPEDANCE MAGNITUDE, Z (Ω)
FREQUENCY, f (Hz)
10^5
10^4
10^3
10^2
10
10^2
10^3
10^4
10^5

Figure 10

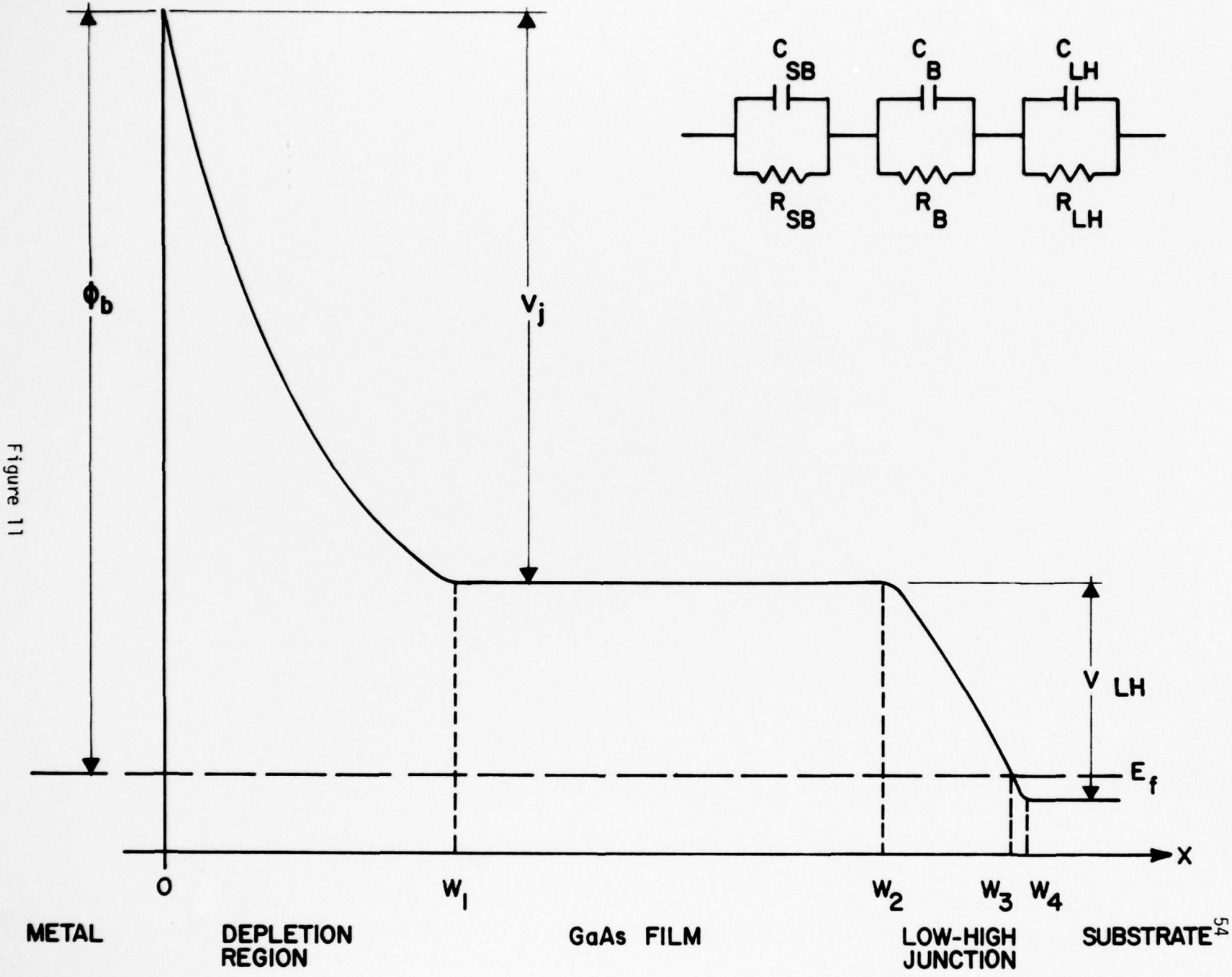
C SB
C B
C LH
R SB
R B
R LH
ϕ_b
V_j
V LH
E_f
X
0
W_1
W_2
W_3
W_4
METAL
DEPLETION REGION
GaAs FILM
LOW-HIGH JUNCTION
SUBSTRATE

Figure 11

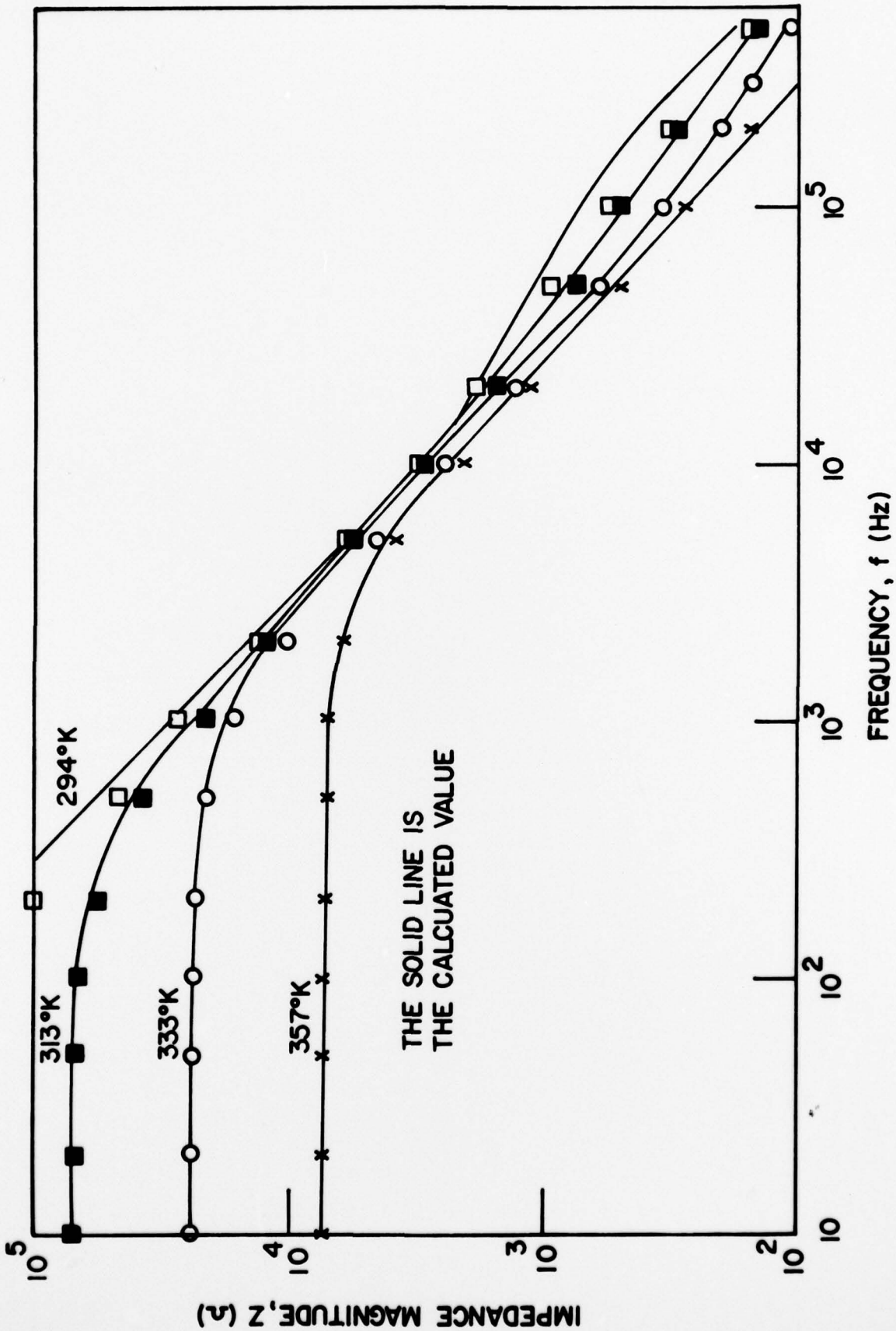
IMPEDANCE MAGNITUDE, Z (Ω)
FREQUENCY, f (Hz)
294°K
313°K
333°K
357°K
THE SOLID LINE IS
THE CALCUATED VALUE

Figure 12

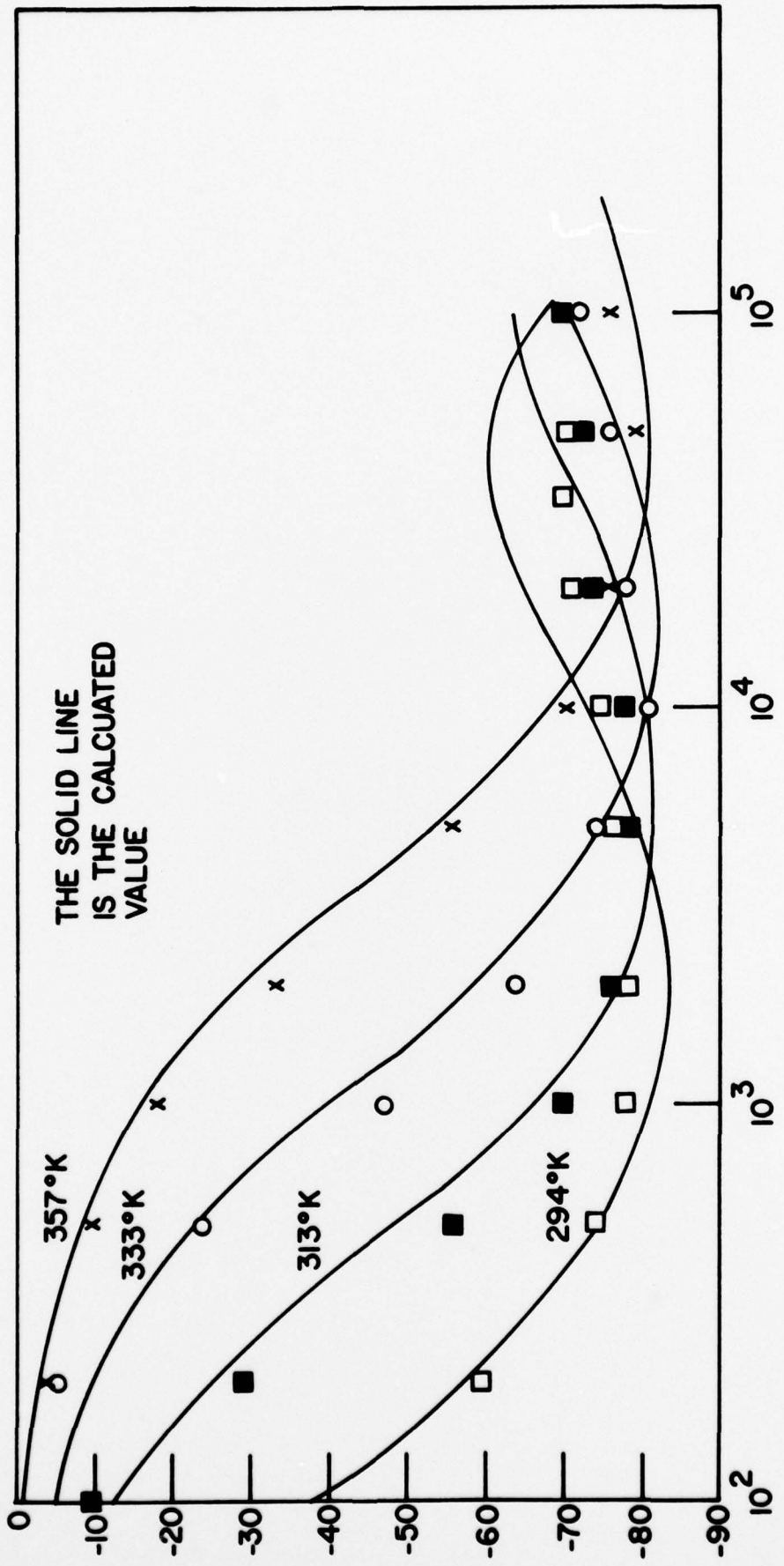
IMPEDANCE PHASE ANGLE, θ°
0
-10
-20
-30
-40
-50
-60
-70
-80
-90
10^2
10^3
10^4
10^5
FREQUENCY, f (Hz)
THE SOLID LINE
IS THE CALCUATED
VALUE
357°K
333°K
313°K
294°K

Figure 13

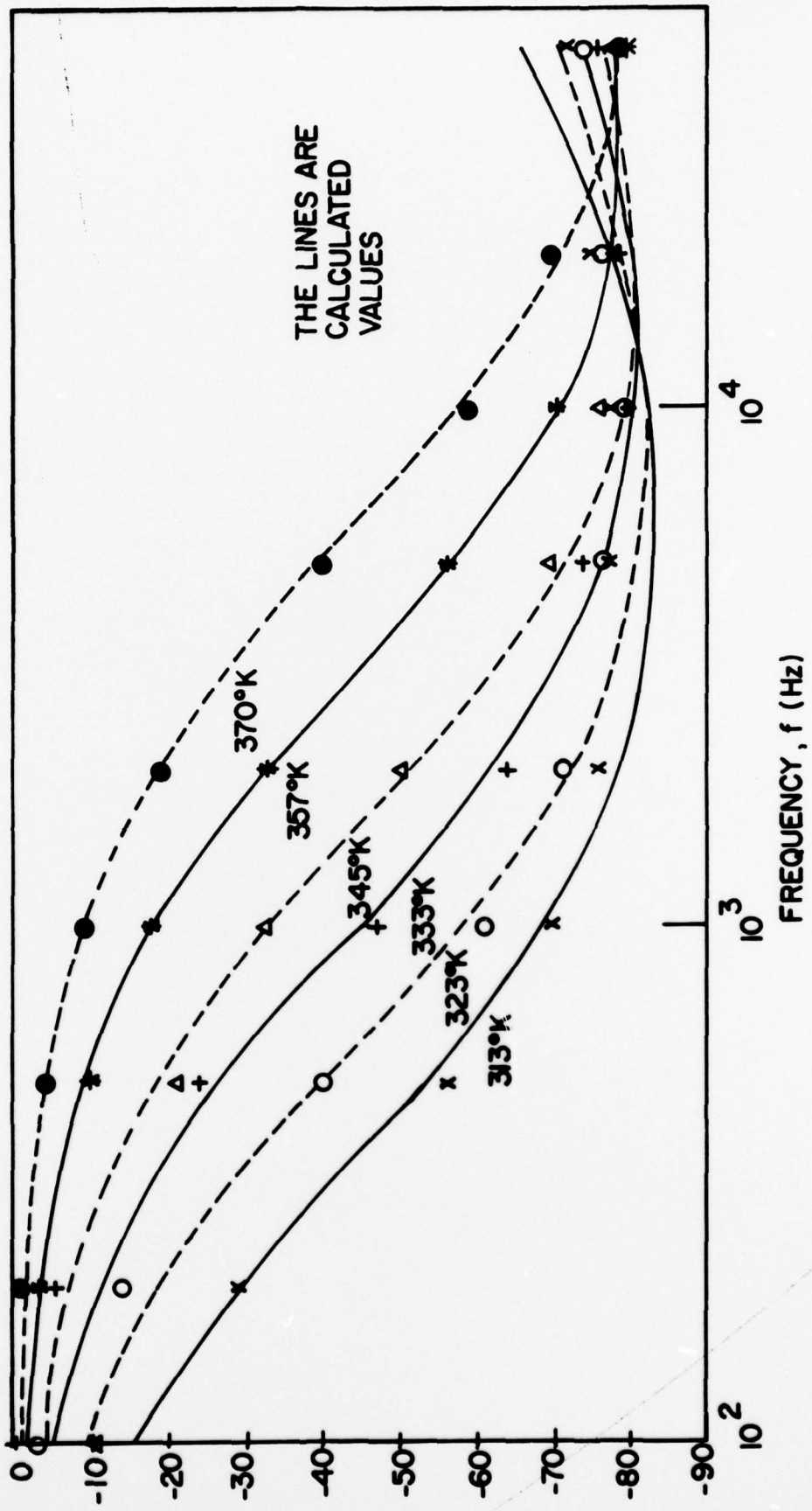
THE LINES ARE CALCULATED VALUES
370°K
357°K
345°K
333°K
323°K
313°K
0
-10
-20
-30
-40
-50
-60
-70
-80
-90
10^2
10^3
10^4
FREQUENCY, f (Hz)
IMPEDANCE PHASE ANGLE, θ°

Figure 14

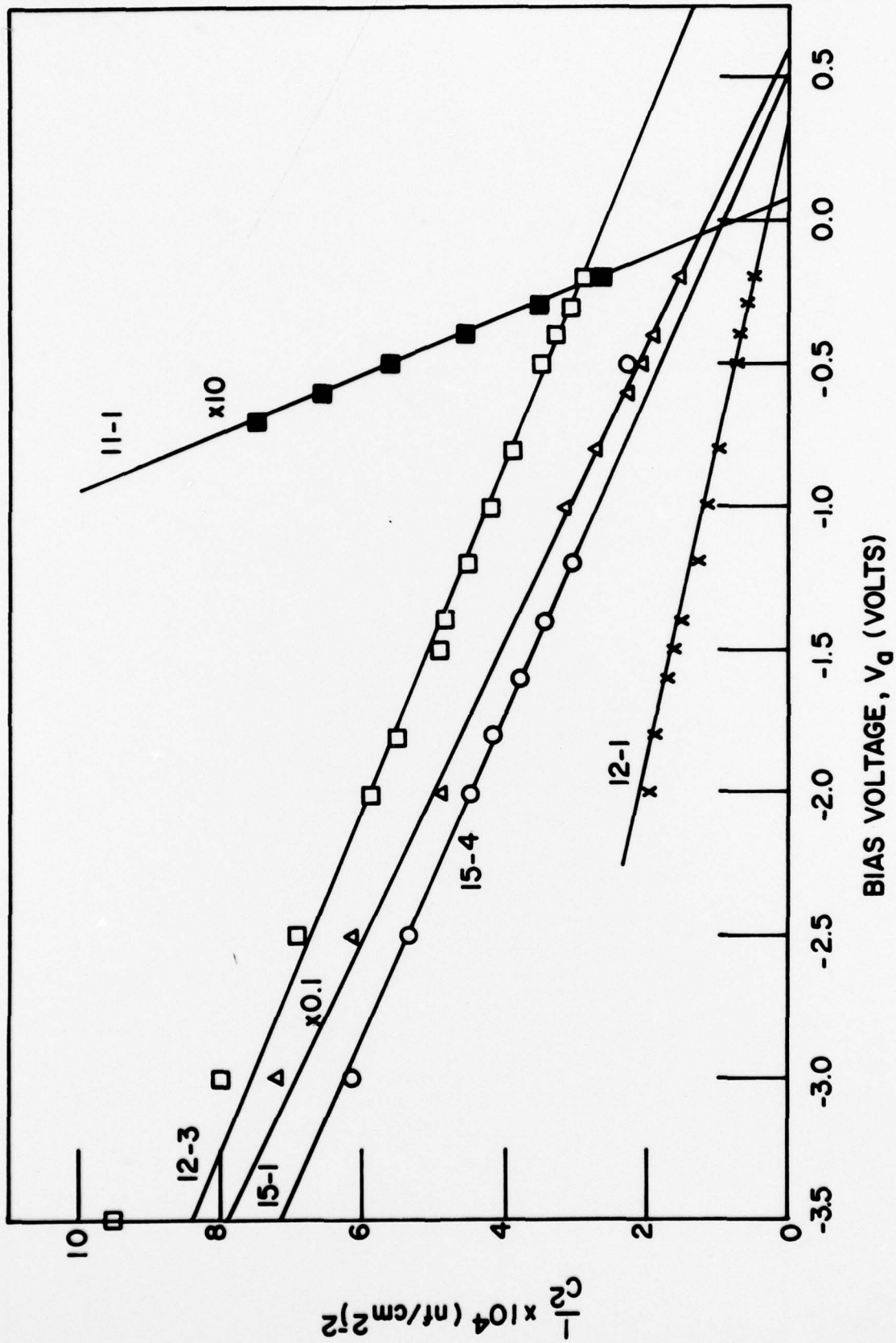
11-1
x10
12-3
x0.1
15-1
15-4
12-1
0.5
0.0
-0.5
-1.0
-1.5
-2.0
-2.5
-3.0
-3.5
BIAS VOLTAGE, V_a (VOLTS)
10
8
6
4
2
0
$\frac{1}{C_d^2} \times 10^4$ (nf/cm^2)^2

Figure 15

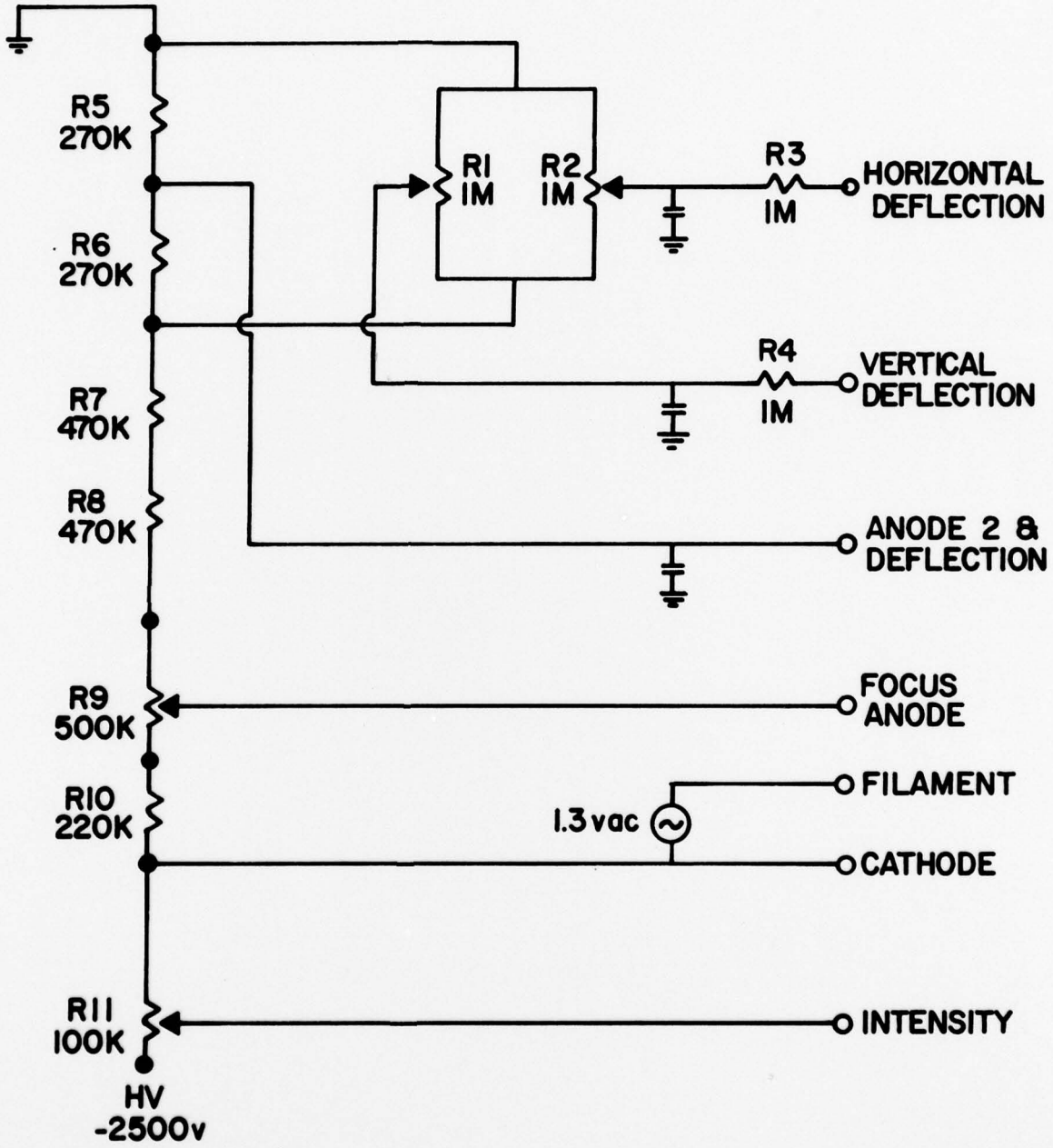
R5
270K
R6
270K
R7
470K
R8
470K
R9
500K
R10
220K
R11
100K
HV
-2500v
R1
1M
R2
1M
R3
1M
HORIZONTAL
DEFLECTION
R4
1M
VERTICAL
DEFLECTION
ANODE 2 &
DEFLECTION
FOCUS
ANODE
FILAMENT
1.3vac
CATHODE
INTENSITY

Figure 16

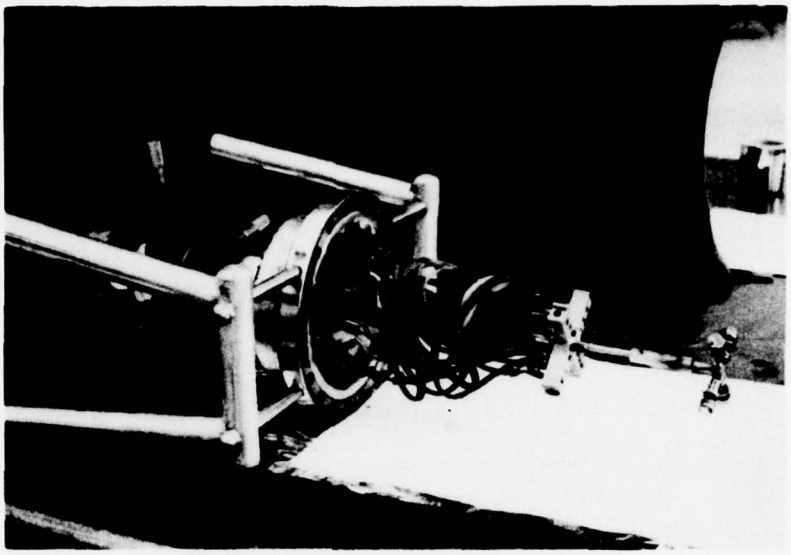

Figure 17

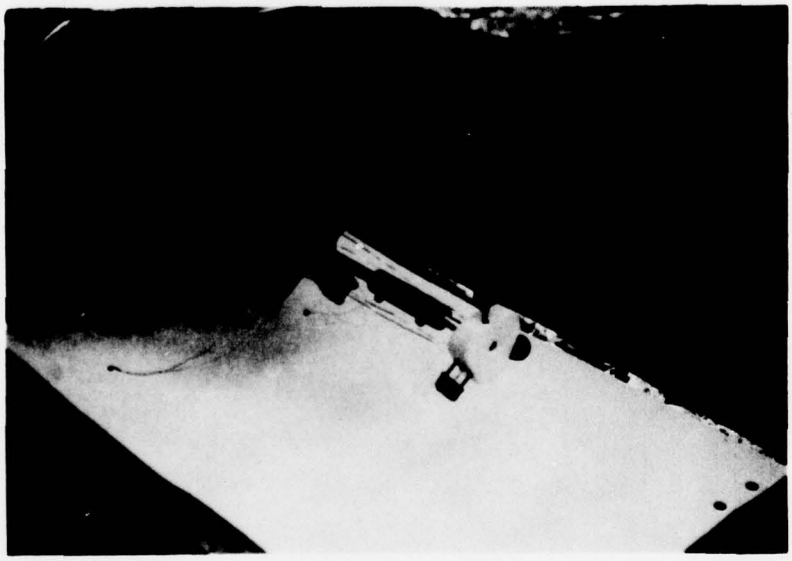

Figure 18

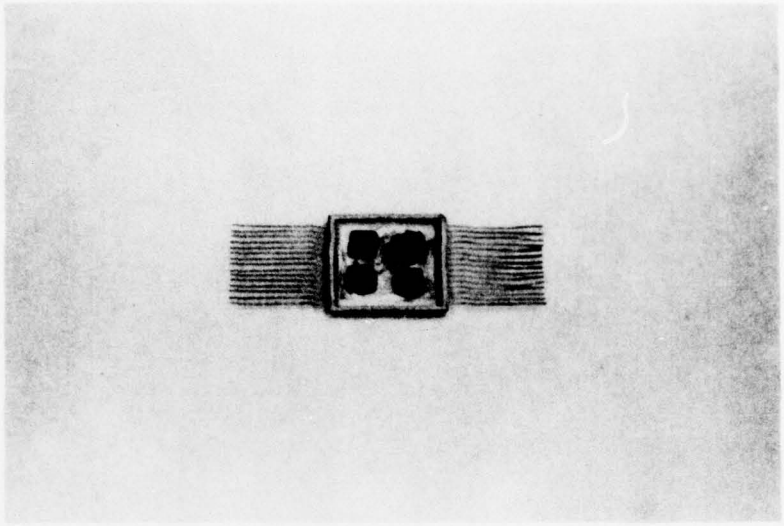

Figure 19

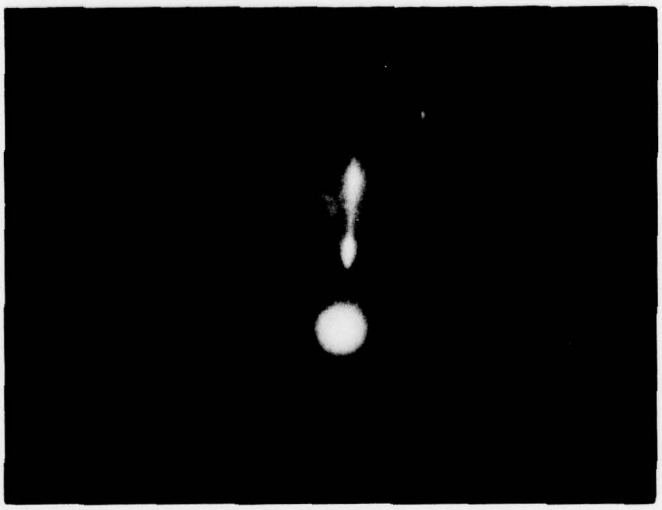

Figure 20

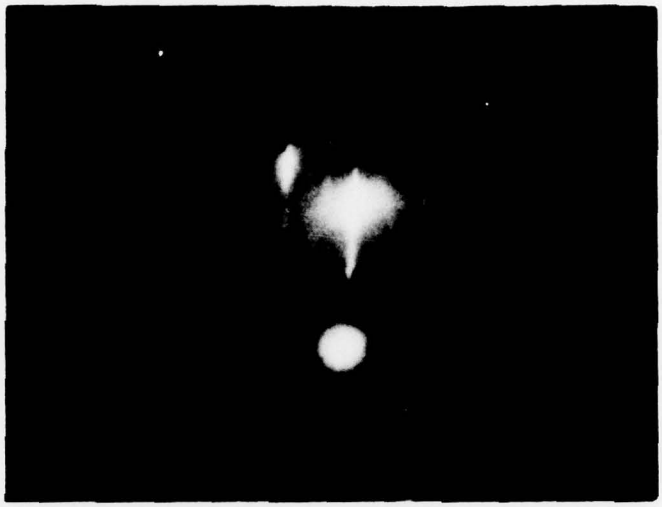

Figure 21

Figure 22

Figure 23

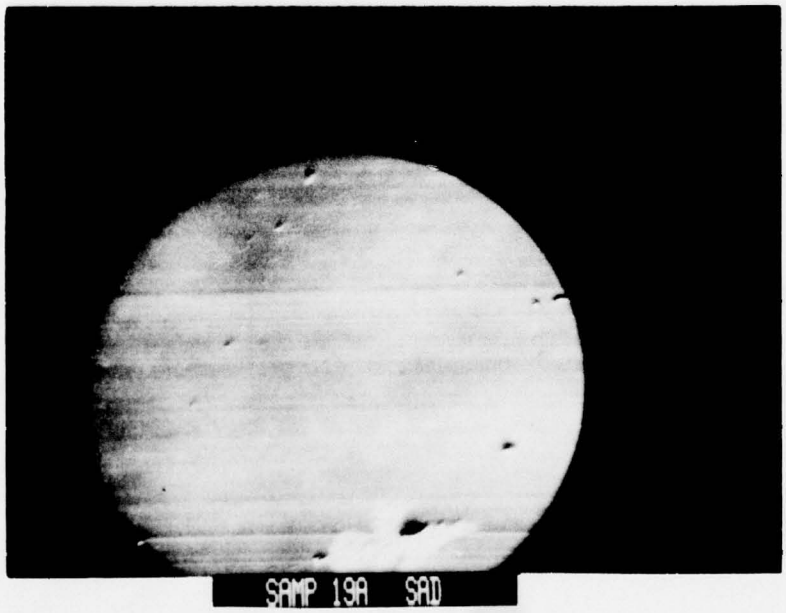

Figure 24